

Beyond maps: Patterns of formation processes at the Middle Pleistocene open-air site of Marathousa 1, Megalopolis Basin, Greece

D. Giusti^{a,*}, V. Tourloukis^a, G. E. Konidaris^a, N. Thompson^a, P. Karkanas^b, E. Panagopoulou^c, K. Harvati^a

^a*Paläoanthropologie, Senckenberg Centre for Human Evolution and Palaeoenvironment, Eberhard Karls Universität Tübingen, Rümelinstr. 23, 72070 Tübingen, Germany*

^b*Malcolm H. Wiener Laboratory for Archaeological Science, American School of Classical Studies at Athens, Greece*

^c*Ephoreia of Palaeoanthropology-Speleology of Greece, Athens, Greece*

Abstract

Recent excavations at the Middle Pleistocene open-air site of Marathousa 1 have unearthed in one of the two investigated areas (Area A) a partial skeleton of a single individual of *Elephas (Palaeoloxodon) antiquus* and other faunal remains in spatial and stratigraphic association with lithic artefacts. In Area B, a much higher number of lithic artefacts was collected, spatially and stratigraphically associated with other faunal remains. The two areas are stratigraphically correlated, the main fossiliferous layers representing an *en masse* depositional process in a lake margin context. Evidence of butchering (cut-marks) has been identified on two bones of the elephant skeleton, as well on other mammal bones from Area B. However, due to the secondary deposition of the main find-bearing units, it is of primary importance to evaluate the degree and reliability of the spatial association of the lithic artefacts with the faunal remains. Indeed, spatial association does not necessarily imply causation, since natural syn- and post-depositional processes may equally produce spatial association. Assessing the degree and extent of post-depositional reworking processes is crucial to fully comprehend the archaeological record, and therefore to reliably interpret past human behaviours. The present study uses a comprehensive set of spatial statistics in order to disentangle the depositional processes behind the distribution of the archaeological and palaeontological record at Marathousa 1. Preliminary results of our analyses suggest minor reworking and substantial spatial association of the lithic and faunal assemblages, supporting the current interpretation of Marathousa 1 as a butchering site.

Keywords: Spatial analysis, Site formation processes, Vertical distribution, Fabric analysis, Point pattern analysis, Middle Pleistocene

*Corresponding author

Email address: domenico.giusti@uni-tuebingen.de (D. Giusti)

1 **1. Introduction**

2 Archaeological site formation processes, intensively studied since the early 1970s
3 ([Isaac, 1967](#); [Schiffer, 1972, 1983, 1987](#); [Shackley, 1978](#); [Wood and Johnson, 1978](#);
4 [Binford, 1981](#); [Schick, 1984, 1986, 1987](#); [Petraglia and Nash, 1987](#); [Petraglia and](#)
5 [Potts, 1994](#), among others), “still insufficiently taken in consideration” ([Texier, 2000](#),
6 p.379) at the beginning of the 21st century, are nowadays fully acknowledged in the ar-
7 chaeological practice ([Villa, 2004](#); [Bailey, 2007](#); [Brantingham et al., 2007](#); [Malinsky-](#)
8 [Buller et al., 2011](#); [Vaquero et al., 2012](#); [Bargalló et al., 2016](#), among others). Drawing
9 inferences about past human behaviours from scatters of archaeological remains must
10 account for syn- and post-depositional contextual processes.

11 Several methods are currently applied in order to qualify and quantify the type and
12 degree of reworking of archaeological assemblages. Within an integrated framework
13 of a geoarchaeological and taphonomic approach, spatial statistics offer meaningful
14 contributions in unravelling site formation and modification processes from spatial pat-
15 terns. However, while the spatio-temporal dimension is an ineluctable inherent prop-
16 erty of any biotic and abiotic process, spatial statistics are still insufficiently applied.

17 Distribution maps are cornerstones of the archaeological documentation process
18 and are primary analytic tools. However, their visual interpretation is prone to subjec-
19 tivity and is not reproducible ([Bevan et al., 2013](#)). Since the early 1970's (see [Hodder](#)
20 and [Orton \(1976\)](#); [Orton \(1982\)](#) and references therein), the traditional, intuitive, ‘eye-
21 balling’ method of spotting spatial patterns has been abandoned in favour of more ob-
22 jective approaches, extensively borrowed from other fields. Nevertheless, quantitative
23 methods, while still percolating in the archaeological sciences from neighbouring dis-
24 ciplines, are not extensively used. Moreover, only a relatively small number of studies
25 have explicitly applied spatial point pattern analysis or geostatistics to the study of site
26 formation and modification processes ([Lenoble et al. \(2008\)](#); [Domínguez-Rodrigo et al.](#)
27 ([2014b,a, 2017](#)); [Carrer \(2015\)](#); [Giusti and Arzarello \(2016\)](#); [Organista et al. \(2017\)](#) -
28 but see [Hivernel and Hodder \(1984\)](#) for an earlier work on the subject).

29 The goal of a taphonomic approach to spatial analysis is to move beyond distri-
30 bution maps by applying a comprehensive set of multiscale and multivariate spatial
31 statistics in order to reliably construct inferences from spatial patterns. An exhaustive
32 spatial analytic approach to archaeological inference, combined with a taphonomic
33 perspective, is essential for evaluating the depositional processes and integrity of the
34 archaeological assemblage, and consequently for a reliable interpretation of past hu-
35 man behaviours.

36 The present study uses a comprehensive set of spatial statistics in order to disentan-
37 gle the depositional processes behind the spatial distribution of the archaeological and
38 palaeontological record recovered during excavation at the Middle Pleistocene open-air
39 site of Marathousa 1, Megalopolis, Greece ([Panagopoulou et al., 2015](#); [Harvati et al.](#),
40 [2016](#)).

41 **1.1. Marathousa 1**

42 The site (Fig. 1), discovered in 2013 at the edge of an active lignite quarry (?), is
43 located between two lignite seams in the Pleistocene deposits of the Megalopolis basin,
44 Marathousa Member of the Choremi Formation ([van Vugt et al., 2000](#)). The regular

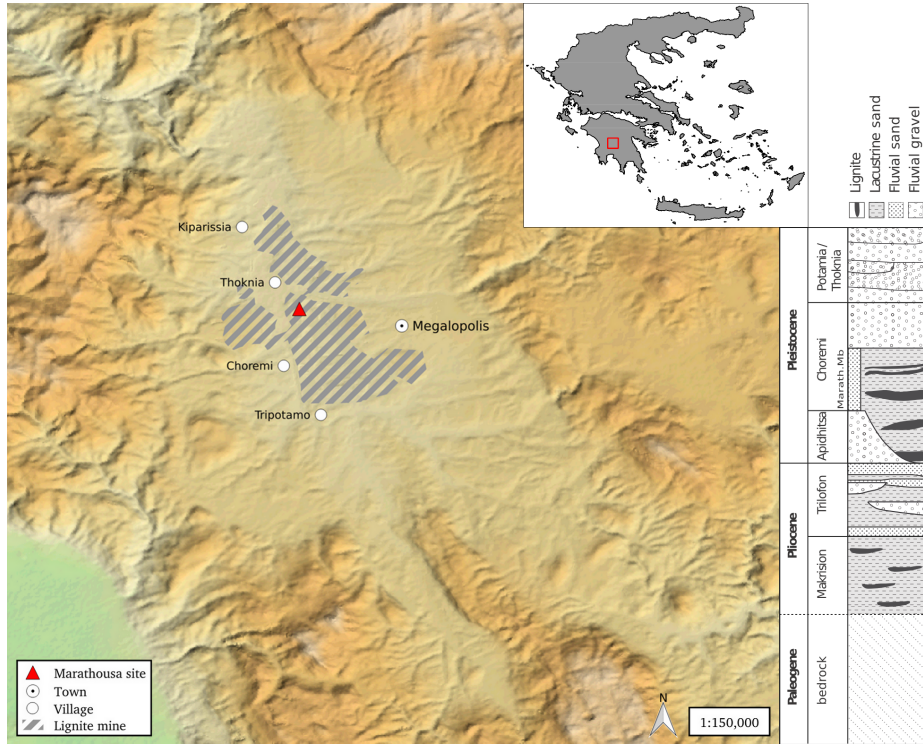


Figure 1: Geographical location of the Marathousa 1 site in the Megalopolis basin and stratigraphic column, modified after [van Vugt et al. \(2000\)](#).

45 alternation of lacustrine clay, silt and sand beds with lignite seams has been interpreted
 46 having cyclic glacial (or stadial) and interglacial (or interstadial) origin ([Nickel et al., 1996](#)). The half-graben configuration of the basin, with major subsidence along the
 47 NW-SE trending normal faults along the eastern margin, resulted in the gentle dip of
 48 the lake bottom at the opposite, western, margin of the lake, enabling the formation of
 49 swamps and the accumulation of organic material for prolonged periods of time ([van
 50 Vugt et al., 2000](#)).

51 Two excavation areas have been investigated since 2013 (Fig. 2): Area A, where
 52 several skeletal elements of a single individual of *Elephas (Palaeoloxodon) antiquus*
 53 have been unearthed, together with a number of lithic artefacts; and Area B, located
 54 60 m to the South along the exposed section, where the lithic assemblage is richer and
 55 occurs in association with a faunal assemblage composed of isolated elephant bones,
 56 cervids and carnivores among others ([Konidaris et al., this issue](#); [Tourloukis et al., this issue](#)). Evidence of butchering (cut-marks) have been identified on two of the
 57 elephant bones from Area A, as well on elephant and other mammal bones from Area
 58 B ([Konidaris et al., this issue](#)).

59 The sedimentary sequence of the site (Fig. 3) includes lacustrine and fluvio-lacustrine
 60 clastic deposits between lignite seam II (UA7-UB10) and the lower part of seam III

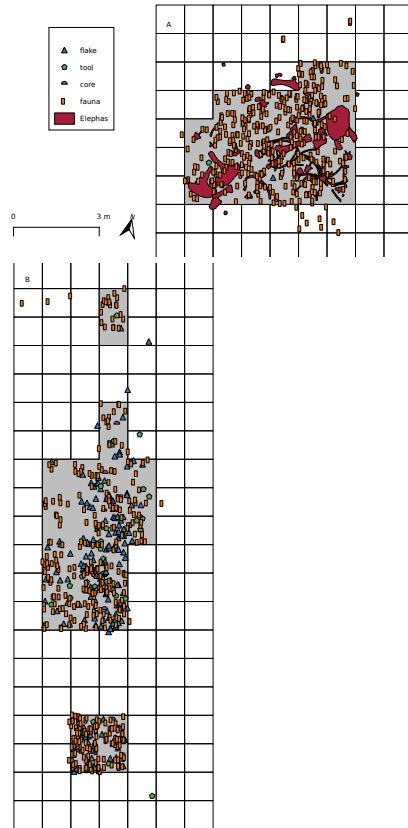


Figure 2: Distribution maps of the remains in Area A and Area B. Grey zone marks the 2015 excavation areas. The two areas are about 60m apart.

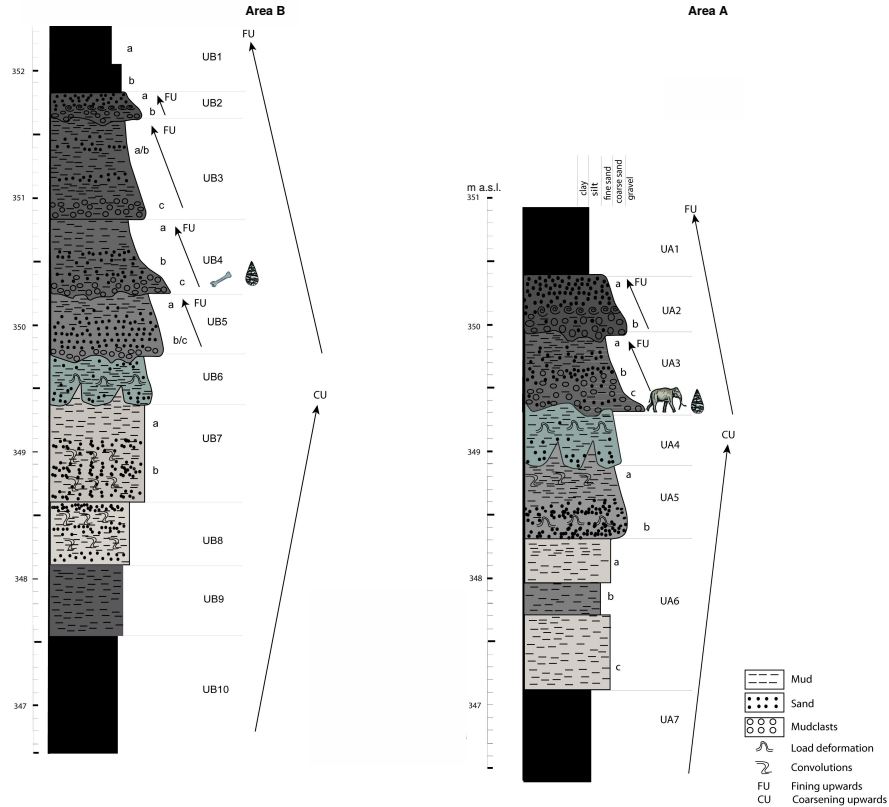


Figure 3: Stratigraphic setting of the Marathousa 1 site, modified after Karkanas et al. (this issue).

(UA1-UB1) (Karkanas et al., this issue; Tourloukis et al., this issue). A major hiatus (UA3/4, UB5/6), attributed to exposure and erosion of a lake shore mudflat, divides the sequence in two parts. The lower part is characterized by relatively high rate subaqueous sedimentation of bedded sands and silts, containing low organic and carbonate content. The upper one is characterized by a series of erosional bounded depositional units, attributed to subaerial organic- and carbonate-rich mudflows and hyperconcentrated flows (Karkanas et al., this issue).

The erosional contacts UA3c/4 and UB4c/5a separate the two main find-bearing units in both areas. In Area A, the elephant remains lie at the contact of UA3c/4 and are covered by UA3c (Fig. 4a); while in Area B, most of the remains were collected from unit UB4c (Fig. 4b). Units UA3c and UB4c (organic- and intraclast-rich silty sands) resemble dilute mudflows, showing a chaotic structure of rip-up clasts from the underlying unit, small-to-large wood fragments and rare rock clasts. In Area B, a relatively low number of remains was also found in massive organic-rich silty sands (UB5a), which locally overlay channalized sands (UB5b/c), probably not preserved in

78 Area A (Karkanas et al., this issue).

79 The flow event described above (units UA3c and UB4c), and specifically the ero-
80 sional contacts between the fossiliferous horizons in the two areas (UA3c/4 and UB4c/5a),
81 provide the essential background for the analysis and interpretation of the spatial dis-
82 tributions at Marathousa 1.

83 The secondary depositional nature of the main find horizons raises the question of
84 how reliable is the spatial association between the lithic artefacts and the partial skele-
85 ton of a single *Elephas (Palaeoloxodon) antiquus* individual and other faunal remains.
86 Since spatial association does not necessarily imply causation, and consequently syn-
87 chrony, the answer has important consequences for the interpretation of the site in the
88 broader context of the Middle Pleistocene human-proboscidean interactions. We aim
89 to tackle this question and disentangle the formation processes acting at Marathousa 1
90 on the basis of spatial patterns through a three-prong spatial analytic approach:

- 91 1. by analysing, in a frame of references, the orientation patterns of remains from
92 relevant stratigraphic units;
- 93 2. by quantifying and comparing their relative vertical distributions;
- 94 3. by identifying spatial trends in either the assemblage intensities and the associa-
95 tions between classes of remains.

96 Two contrasting hypotheses are tested: the autochthonous model (Fernández-López,
97 1991; Domínguez-Rodrigo et al., 2012, sensu) states that the flow event, represented
98 by units UA3c and UB4c, eroded and scoured the exposed surface (where the elephant
99 was lying), thereby entraining clastic material (including artefacts) and re-depositing
100 (Fernández-López, 1991, sensu) this material at a close distance. This model implies
101 the loss of any original, pristine spatial relations between remains, but minor trans-
102 port from the primary depositional *loci*. On the other hand, the allochthonous model
103 (Fernández-López, 1991; Domínguez-Rodrigo et al., 2012, sensu) implies significant
104 transport from the original *loci* of deposition and re-elaboration (Fernández-López,
105 1991, sensu). According to this model, the spurious spatial association between the
106 lithic artefacts and faunal remains does not support any behavioural interpretation.

107 2. Material and methods

108 Since 2013, systematic investigation of the Marathousa 1 site has been carried out
109 by a joint team from the Ephoreia of Palaeoanthropology-Speleology (Greek Ministry
110 of Culture) and the University of Tübingen. A grid system of 1 square meter units
111 was set up, oriented -14 degrees off the magnetic North, and including the two areas
112 of investigation. The excavation of the deposit proceeded in 50x50 cm sub-squares
113 in Area B and 1x1 m squares in Area A, and spits of 5 to 10 cm thickness, respec-
114 tively. Systematic water-screening of sediments was carried out on-site using 1 mm
115 sieves in order to guarantee recovery of the small-size fraction (e.g., micro-artefacts,
116 small mammal remains, fish, molluscs and small fragments of organic and inorganic
117 material). The three-dimensional coordinates of finds (i.e., all the lithic artefacts, teeth
118 and diagnostic bones; bones and organic material with a-axis \geq 20 mm), collected
119 spits of sediment, samples and geological features (e.g., erosional contacts and mud



Figure 4: Photograph (2017) of the left femur of the *Elephas (Palaeoloxodon) antiquus*, lying at the contact of UA3c/4 and covered by UA3c (a). West profile (2014) of the excavation Area B, exposing the UB4c/5a and UB5c/6 erosional contacts (b).

120 cracks) were recorded with a Total Station. Dense clouds of surface points of the Elephant skeletal elements were acquired using both a Total Station and a close-range
121 photogrammetric technique.
122

123 The dimensions (length, width and thickness) of registered finds were measured
124 on-site with millimetre rules. Orientation (dip and strike) of elongated particles (i.e.,
125 faunal remains, large wood fragments and lithic artefacts) was recorded since 2013
126 with a 30 degree accuracy, using a clock-like system (the strike was measured, rela-
127 tively to the grid North, in twelve clockwise intervals). In 2015, the use of a compass
128 and inclinometer with an accuracy of 1 degree was introduced in Area B to gradually
129 replace the former method.

130 The widespread use of a compass and inclinometer to record orientation data (Voorhies,
131 Fiorillo, 1991; Bertran and Texier, 1995; Bertran et al., 1997; Lenoble and
132 Bertran, 2004; Eberth et al., 2007; Eren et al., 2010; Benito-Calvo et al., 2011; Domínguez-
133 Rodrigo et al., 2012; Domínguez-Rodrigo and García-Pérez, 2013; Domínguez-Rodrigo
134 et al., 2014c; Cobo-Sánchez et al., 2014; Organista et al., 2017, among others) was
135 favoured over the alternative use of a total station (Klusken, 1990; Dibble et al., 1997;
136 McPherron, 2005; Enloe, 2006; Bernatchez, 2010, among others), mostly due to the
137 time-restricted conditions of the rescue excavation conducted at Marathousa 1.

138 Measurements of the strike (azimuth) and dip of elongated finds were taken along
139 the symmetrical longitudinal a-axis (SLA) of bones (Domínguez-Rodrigo and Garcí-
140 Pérez, 2013), lithic artefacts (Bertran and Texier, 1995) and wood fragments (Macdon-
141 ald and Jefferson, 1985), using the lowest endpoint of the axis as an indicator of the
142 vector direction.

143 Other major axes have been alternatively used with the recent application of GIS
144 techniques to retrieve orientation data from secondary source (i.e., excavation pho-
145 tographs, drawings or maps) (Boschian and Saccà, 2010; Benito-Calvo and de la Torre,
146 2011; de la Torre and Benito-Calvo, 2013; Walter and Trauth, 2013; García-Moreno
147 et al., 2016; Sánchez-Romero et al., 2016). However, the experimental works of Domínguez-
148 Rodrigo and García-Pérez (2013) and Domínguez-Rodrigo et al. (2014c) showed that
149 the SLA, defined as the major axis which symmetrically divide the bone, is more accu-
150 rate in determining the preferential orientation of anisotropic assemblages. This a-axis
151 is commonly used in taphonomic studies (Toots, 1965; Voorhies, 1969; Eberth et al.,
152 2007; Domínguez-Rodrigo et al., 2012, 2014a; Aramendi et al., 2017, among others)
153 and, commonly referred to as the clast/artefact long or major axis (Krumbein, 1941),
154 in studies which employ a sedimentological approach to archaeological fabric (Bertran
155 and Texier, 1995; Bertran et al., 1997; Lenoble and Bertran, 2004; Benito-Calvo et al.,
156 2009, among others).

157 The present study focuses on the excavated stratigraphic units in which most of the
158 archaeological and palaeontological remains were recovered in both excavation areas,
159 namely in UA3c and UA4 in Area A, and UB4c and UB5a in Area B. From the total,
160 subset samples of material were used for each specific spatial analysis. For the fabric
161 analysis we included material collected until 2016. For the vertical distribution and
162 point pattern analyses, the region of investigation was limited to the squares excavated
163 from 2013 until 2015, 25 and 29 square meters respectively in each area.

164 The analyses were performed in R statistical software (R Core Team, 2016). In
165 order to make this research reproducible (Marwick, 2017; Marwick et al., 2017), a

repository containing a compendium of data, source code and text is open licensed and available at the DOI: [10.5281/zenodo.822273](https://doi.org/10.5281/zenodo.822273)

2.1. Fabric analysis

The study of the clast fabric (i.e., the orientation pattern of elongated sedimentary particles, including bones and artefacts), first addressed by Voorhies (1969); Isaac (1967); Bar-Yosef and Tchernov (1972); Schick (1986), more recently led to a noteworthy development of methods and propagation of applications in Palaeolithic site formation studies (Bertran and Texier, 1995; Bertran et al., 1997; Lenoble and Bertran, 2004; Lenoble et al., 2008; McPherron, 2005; Benito-Calvo et al., 2009, 2011; Benito-Calvo and de la Torre, 2011; Bernatchez, 2010; Boschian and Saccà, 2010; Domínguez-Rodrigo et al., 2012; Domínguez-Rodrigo and García-Pérez, 2013; Domínguez-Rodrigo et al., 2014c; de la Torre and Benito-Calvo, 2013; Walter and Trauth, 2013; García-Moreno et al., 2016; Sánchez-Romero et al., 2016, among others).

Fabric analysis can provide valuable insight into site formation and taphonomic processes, allowing discrimination between orientation patterns (isotropic, linear or planar) associated with different sedimentary processes. Whereas water-flow deposits are, in general, characterized by relatively good sorting and preferred orientation of clasts parallel, or normal to the flow direction (linear fabric) (Petricola and Potts, 1994); debris-flow deposits generally exhibit massive, poorly bedded mixtures of unsorted sediments and random orientation of clasts (isotropic fabric), except at the flow margins (Pierson, 2005). On the other hand, undisturbed archaeological sites, as well as experimental sites, have been observed to have planar fabric (Bertran et al., 1997; Lenoble and Bertran, 2004). Nevertheless, grey zones exist between depositional processes, so that an unequivocal discrimination based only on fabric observations is often not possible, and other taphonomic criteria must also be considered (Lenoble and Bertran, 2004). As an example, while overland flows (runoff) have been observed to show planar fabrics (Lenoble and Bertran, 2004), anisotropy without significant transport can be caused in a lacustrine floodplain by low-energy processes such as lake transgression and regression, as well as water-sheet flows formed during rainy seasons (Cobo-Sánchez et al., 2014).

At the margin of a lacustrine environment, relatively close to the surrounding relief, a combination of high- and low-energy processes can be expected. According to the sedimentological and micromorphological study of the Marathousa 1 site, mudflows and hyperconcentrated flows are associated with the main find-bearing horizons (Karkanas et al., this issue). Hyperconcentrated flows are intermediate states, defined by sediment concentration, in the continuum between subaerial water flows and debris flows. Benvenuti and Martini (2002) report that, when a turbulent fluidal flow expands over a surface - as in the case of Marathousa 1 - a two-phase flow may develop, with a more concentrated, coarser grained bottom flow-layer (traction carpet) moving slower than the upper turbulent flow-layer carrying washload and suspended load. Resultant deposit may exhibit diagnostic inverse grading, or a continuously aggrading bed. Parallel or normal orientation of the clast to the flow direction can be observed (Benvenuti and Martini, 2002). Moreover, a simulation model showed that linear fabric can develop in mudflows as well. However, after deposition, settling of the clasts may affect the fabric to some extent, depending on the viscosity of the mudflow (Lindsay, 1968).

Table 1: List of sampled observations for the fabric analysis.

Sample	<i>n</i>	Type		
		Fauna	Wood	Lithic
UA3c	49	23	25	1
UA4	38	8	30	-
<i>E. (P.) antiquus</i>	63			
UB4c	38	30	1	7

211 As part of our three-prong spatial analytic approach, we conducted comparative
 212 fabric analysis with the aim to investigate the dynamics of the depositional processes
 213 at Marathousa 1.

214 Since fabric strength has been found to be positively correlated with the shape and
 215 size of the clast, for the fabric analysis we subset samples of remains with length ≥ 2 cm
 216 and elongation index (the ratio length/width) $I_e \geq 1.6$ (Lenoble and Bertran, 2004). The
 217 samples are listed in Table 1 and include mostly wood fragments and faunal remains
 218 from the four stratigraphic units under investigation. Bones have been found to readily
 219 react to water flow and show very early anisotropic patterns (Schick, 1984; Domínguez-
 220 Rodrigo et al., 2014c). Flume experiments showed that wood fragments as well tend to
 221 align parallel to the current direction (Macdonald and Jefferson, 1985). No distinction
 222 of skeletal elements was made, both due to the high fragmentation rate of faunal re-
 223 mains in Area B, and because recent experiments showed a similar orientation pattern
 224 for different bone shapes (Domínguez-Rodrigo et al., 2012; Domínguez-Rodrigo and
 225 García-Pérez, 2013).

226 The sample of bones belonging to the individual of *Elephas (P.) antiquus* from
 227 Area A was analysed separately and included the humerus, ulna, femur and tibia; the
 228 atlas, axis and 16 complete vertebrae or vertebral fragments; 29 complete ribs or rib
 229 fragments; 2 calcanea; 4 metatarsals/metacarpals; the pyramidal; the trapezoid and the
 230 pelvis. The sample from UB5a was too small (only 7 observations) and was therefore
 231 excluded. In order to asses the reliability of the orientation data recorded using the
 232 clock method, we analysed two sub-samples from unit UB4c, selected from a set of
 233 finds recorded using both methods. All the sampled observations are representative of
 234 the whole study area.

235 Rose diagrams and uniformity tests, such as Rayleigh, Kuiper, Watson and Rao
 236 tests (Jammalamadaka et al., 2001), were used to visualise and evaluate circular isotropy
 237 in the sample distribution. The Rayleigh test is used to assess the significance of the
 238 sample mean resultant length (\bar{R}), assuming that the distribution is unimodal and not
 239 bi- or plurimodal. The \bar{R} ranges from 0 to 1: values close to 1 indicate that the data are
 240 closely clustered around the mean direction; when the data are evenly spread \bar{R} has a
 241 value close to 0. A p -value lower than 0.05 rejects the hypothesis of randomness with
 242 a 95% confidence interval. Kuiper, Watson and Rao are omnibus tests used to detect
 243 multimodal departures from circular uniformity. The Watson's goodness of fit test was
 244 conducted for the von Mises distribution (circular normal distribution). The test results
 245 are evaluated against critical values: a result higher than the critical value rejects with
 246 confidence the null hypothesis.

247 Randomness testing of three-dimensional data was conducted with the Woodcock

248 S_1/S_3 test (Woodcock and Naylor, 1983). Considering both the dip (plunge) and strike
249 (bearing) of the oriented items, this method, based on three ordered eigenvalues (S_1 ,
250 S_2 , S_3), is able to discriminate the shape and strength of the distributions. The shape
251 parameter $K = \frac{\ln(S_1/S_2)}{\ln(S_2/S_3)}$ ranges from zero (uni-axial girdles) to infinite (uni-axial clus-
252 ters). The parameter $C = \ln(S_1/S_3)$ expresses the strength of the preferential orien-
253 tation, and its significance is evaluated against critical values from simulated random
254 samples of different sizes. A perfect random uniform distribution would have $C = 0$
255 and $K = 1$.

256 The Benn (Benn, 1994) diagram adds to the Woodcock test an isotropy ($IS =$
257 S_3/S_1) and an elongation ($ES = 1 - (S_2/S_1)$) index. Like the former method, it is
258 able to differentiate between linear (cluster), planar (girdle) or isotropic distributions.
259 There are no published raw data from actualistic studies on hyperconcentrated flows or
260 other depositional processes affecting the orientation of bones and artefacts deposited
261 on lacustrine floodplains (but see Morton (2004) and Cobo-Sánchez et al. (2014) as
262 pioneer studies on this subject). However, we included in the Benn diagram references
263 to published results from observation of fabrics in modern subaerial slope deposits,
264 i.e., debris flow and runoff (Bertran et al., 1997; Lenoble and Bertran, 2004).

265 2.2. Vertical distribution

266 The vertical distribution of materials has been long investigated with the aim of
267 identifying cultural levels, by visually interpreting cross-sectional plots. However, re-
268 cent advances in GIS techniques allow to quantitatively inspect at higher resolution
269 the three-dimensional distributions of archaeological remains (McPherron et al., 2005;
270 Anderson and Burke, 2008, among others).

271 In analysing the vertical dispersion of material at Marathousa 1, we provisionally
272 assume that a general concentration of unsorted lithic artefacts and faunal remains in
273 the proximity of the erosional surfaces would support an autochthonous origin of the
274 assemblages; whereas a homogeneous vertical distribution of remains from the UA3c
275 and UB4c units would suggest an allochthonous origin, significant transport and sub-
276 sequent redeposition of the material. Indeed, massive process such as mudflows or hy-
277 perconcentrated flows, have high erosional power and rather chaotic structure, which
278 may result in inverse or normal grading (Benvenuti and Martini, 2002).

279 In order to estimate the degree of vertical dispersion while controlling for the size
280 of the archaeological material, dimensional classes were set up following typological
281 criteria. Lithic artefacts were classified as debris/chips when smaller than a cutoff
282 length of 15 mm (see Tourloukis et al. (this issue)). Other classes include flakes, tools
283 and cores; the latter being the bigger and heavier debitage product. Table 2 summarises
284 the sample size for each class. Lithic debris/chips constitutes the larger part of the
285 assemblages from UB4c (60%) and UB5a (49%); whereas in Area A it represents only
286 a moderate percentage in the upper UA3c unit (16%). The very rare presence of lithic
287 artefacts in the underlying unit UA4 is nevertheless significant. In this unit, the faunal
288 remains are also found in much lower numbers, their number reduced to one fourth
289 of those found in UA3c. For the point pattern analysis (see below), we used the same
290 subset of materials for both excavation areas.

291 For Area B, the material recovered from the water-screening was randomly pro-
292 venance according to the 5 cm depth of the excavated spit and the coordinates of the

Table 2: List of sampled observations for the vertical distribution and point pattern analyses.

Sample	<i>n</i>	Lithic class					Faunal class			
		Debris/chip	Flake	Bone flake	Tool	Core	Indet.	Bone	Tooth	Microfauna
UA3c	279	46	2	-	1	-	1	171	14	44
UA4	61	3	1	-	-	-	-	45	4	8
UB4c	1243	753	154	1	34	6	2	246	28	19
UB5a	101	50	12	-	3	-	-	30	3	3

50x50 cm quadrant of the excavation square. Following the same excavation protocol, the same procedure was applied for the water-screened material of Area A, which was randomly provenanced according to 3D-coordinates of the 1x1 m excavation square and 10 cm spit.

Ordinary Kriging interpolation of the recorded points of contact between the UA3c/UA4 and UB4c/UB5a stratigraphic units were used to reconstruct the UA3c/4 and UB4c/5a erosional surface (Fig. 5a,b). In geostatistics, Kriging is a method of interpolation which, from a modelled function of spatial autocorrelation between known points (e.g., recorded elevations), calculates values of unknown points (e.g., predicted elevations). Thus, in order to address our specific objective, i.e., to quantify and analyse the vertical distribution of the archaeological and palaeontological material, we measured the minimum orthogonal distance of each specimen to the interpolated erosional surface (Fig. 5c). For the units above and below this surface (i.e., UB4c and UB5a), the relative distribution of lithic classes and faunal remains was informally tested by means of kernel density estimations.

In Area A, the UA3c/4 erosional surface is mixed, rather than sharp: remains of the eroded unit UA4 are mixed with pockets of the UA3c organic-rich silty sands and intraclast-rich mudflows (Karkanas et al., this issue). However, from sparse known points of the erosional contact, the UA3c/4 surface was interpolated and the vertical dispersion of remains estimated. The elephant remains were excluded from this analysis, since they clearly lie horizontally at the UA3c/4 contact (Fig. 4a and SI).

Finally, a Student's two sample t-test allowed us to compare the empirical distributions of different groups of remains for each stratigraphic unit.

2.3. Point pattern analysis

A spatial point pattern is defined as the outcome of a random spatial point process (repetitions of it would always create a different pattern). The observed patterns of the archaeological and palaeontological remains were treated as manifestations of spatial point processes, i.e., site formation processes. Point pattern analysis investigates the spatial arrangement of points with the aim of identifying spatial trends. In order to integrate the previous studies of the fabric and vertical distributions, we directed our point pattern analysis equally to the intensity of the patterns (the rate of occurrence of the recorded finds) and to the spatial interaction between different types of finds.

As the average number of random points per unit area, intensity informs about homogeneity or inhomogeneity in the distribution of events generated by a point process, i.e., whether the rate of occurrence is uniform or spatially varying across the study area. Intensity, usually non-parametrically evaluated by means of kernel density estimation

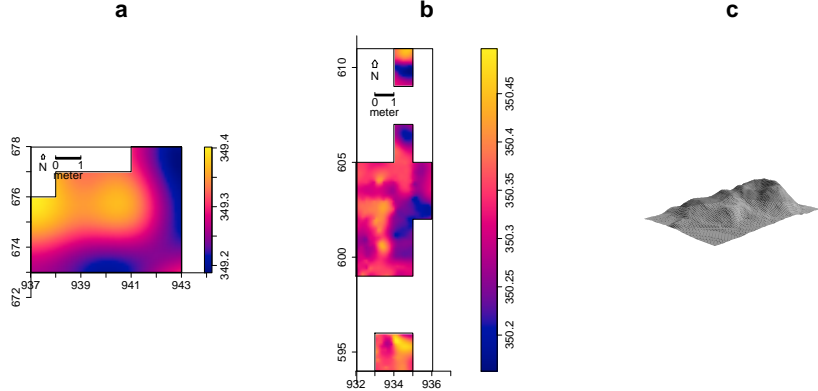


Figure 5: Ordinary Kriging interpolation of the UA3c/4 (a) and UB4c/5a (b) erosional surface; the color scale denotes elevation a.s.l. Illustration of the method used to quantify the vertical dispersion of remains with respect to the UB4c/5a surface (c).

(Diggle, 1985), was assessed for the distribution of material from the UB4c, UB5a and UA3c units. Cross-validation bandwidth, which assumes a Cox process, and edge correction were applied using the methods described in Diggle (1985).

In the presence of a covariate, it is recommended to further investigate the dependence of intensity on that explanatory variable. In order to evaluate whether variation in the density of materials was correlated to the topography of the erosional surface, we computed a local likelihood smoothing estimate of the intensity of remains from UB4c as a function of the UB4c/5a surface elevation model (Baddeley et al., 2012). Formal tests enabled us to assess the evidence of that dependence and to quantify the strength of the covariate. The Kolmogorov-Smirnov test of CSR (Complete Spatial Randomness) and Berman's Z_2 statistics were used to test the strength of evidence for a covariate effect. The Receiver Operating Characteristic (ROC) plot, and the area under the ROC curve (AUC), closely related to Berman's Z_2 test, measure the magnitude of the covariate effect. AUC values close to 1 or 0 indicate strong discrimination, whereas intermediate values (0.5) suggest no discrimination power.

Intensity, although informative and widely evaluated by means of kernel density maps, nonetheless provide sufficient information to reliably infer about site formation processes.

Whereas intensity is a first-order property of the point process, multiscale inter-point interaction is measured by second or higher-order moment quantities, such as the Ripley's K correlation function (Ripley, 1976, 1977) and the distance G -, F - and J -functions. Three different types of inter-point interaction are possible: random, regular or cluster. In a hypothesis-testing framework, pointwise envelopes are computed by a number of random simulations of the null hypothesis (i.e., random/Poisson distribution). Thus, values of the empirical distribution (black solid line) are plotted against the benchmark value (red dotted line) and the envelopes (grey area) which specify the

critical points for a Monte Carlo test (Ripley, 1981). Regular patterns are assumed to be the result of inhibition processes, while cluster patterns are the result of attraction processes.

In order to test the spatial interaction between remains associated with the erosional event of UB4c and those associated with the underlying UB5a unit, we treated the data as a multivariate point pattern, assuming that the point patterns in UB4c and UB5a are expressions of two different stationary point processes, i.e., depositional events. We performed a cross-type pair correlation function ($g_{ij}(r)$), derivative of the multitype $K_{ij}(r)$ function, which is the expected number of points of type j lying at a distance r of a typical point of type i . The function is a multiscale measurement of the spatial dependence between types i (UB4c) and j (UB5a). Randomly shifting in 199 Monte Carlo permutations each of the two patterns, independently of each other, estimated values of $\hat{g}_{ij}(r)$ are compared to a benchmark value $g_{ij}(r) = 1$, which is consistent with independence or at least with lack of correlation between the two point processes. In order to reduce the edge effect bias in estimating the correlation between points, we implemented Ripley's isotropic edge correction (Ohser, 1983; Ripley, 1988).

In addition to the pair correlation function, the multitype nearest-neighbour $G_{ij}(r)$ function was used to estimate the cumulative distribution of the distance from a point of type i (UB4c) to the nearest point of type j (UB5a). It measures the spatial association between the two assemblages. For the cross-type G -function, the null hypothesis states that the points of type j follow a Poisson (random) distribution in addition to being independent of the points of type i . Thus, in a randomisation technique, when the solid line of the observed distribution ($\hat{G}_{ij}(r)$) is above or below the shaded grey area, the pattern is significantly consistent with clustering or segregation, respectively.

Complete spatial randomness and independence (CSRI) of the two point processes (UB4c and UB5a) would support an allochthonous origin hypothesis for the assemblage recovered from the UB4c unit. According to the allochthonous model, the massive, chaotic UB4c flow event re-elaborated and randomly deposited the embedded material. On the other hand, positive or negative association can be interpreted as expression of different autochthonous processes.

The particle size horizontal distribution of the lithic assemblage from UB4c was investigated by means of a transformation of the multitype K -function ($K_{i\bullet}(r) - K(r)$, see Baddeley et al. (2015), p.608). In this case, we treated the data as the manifestation of a single multitype point process. In a joint distribution analysis, the locations and types of points are assumed to be generated at the same time. The null model of a random labelling test states that the type of each point is determined at random, independently of other points, with fixed probabilities. The estimated K -function for a subset of possible combinations was evaluated against the envelope of 199 Monte Carlo permutations of the class of remains.

Whereas the null hypothesis of the randomness is consistent with an allochthonous model, spatial clustering or segregation would support an autochthonous model. Specifically, horizontal clustering of small specimens, such as lithic debris/chips, together with larger dimensional classes of remains would suggest the lack of sorting by natural depositional processes predating the UB4c flow event, when the UB5a surface was exposed to erosion. On the other hand, spatial segregation would suggest the action of sorting processes, such as winnowing.

Table 3: Value and p – value of circular uniformity test statistics.

Sample	mean dir.	Rayleigh		Kuiper		Watson		Rao	
		R	p	V_n	p	U^2	p	U	p
UA3c	77.17°	0.268	0.029	2.4698	<0.01	0.2967	<0.01	271.8367	<0.001
UA4	35.79°	0.386	0.003	2.5656	<0.01	0.3437	<0.01	246.3158	<0.001
<i>E. (P.) antiquus</i>	54.64°	0.489	2.775e-07	3.4811	<0.01	0.906	<0.01	291.4286	<0.001
UB4c (clock)	83.96°	0.167	0.091	2.327	<0.01	0.2466	0.01 < p < 0.025	309.7674	<0.001
UB4c (compass)	128.14°	0.225	0.037	1.6917	0.05 < p < 0.10	0.1862	0.05 < p < 0.10	153.3846	0.01 < p < 0.05

401 As for the three-dimensional distribution of the lithic artefacts in Area A, and their
402 spatial association with the partial skeleton of the *E. (P.) antiquus*, we applied three-
403 dimensional univariate and bivariate second-order functions. A rectangular box of 20
404 square meters and 80 cm vertical extent was selected for the analyses (green outline in
405 Fig. 11a). Assuming homogeneity, the univariate pair correlation function ($g_3(r)$) was
406 estimated for the pattern of all the artefacts (mostly debris/chips) from UA3c and UA4.

407 In the specific context of the site, complete spatial randomness (CSR) would sug-
408 gest that the pattern most probably is the result of a random distribution process, such
409 as a high energy mass movement, thus supporting an allochthonous model. In contrast,
410 other natural processes would produce clustering or segregation of the lithic artefacts.
411 Spatial aggregation, if not generated by obstructions, would support an autochthonous
412 origin of the assemblage.

413 In support to the pair correlation function, the cross-type nearest-neighbour func-
414 tion has been applied in order to compute, for each artefact recovered from the UA3c
415 and UA4 units, the nearest point of the clouds of points associated with the elephant
416 skeleton. A prevalence of short distances would indicate aggregation of the lithic arte-
417 facts around the mass of the elephant; whereas a uniform or symmetric distribution
418 would support random independent processes.

419 3. Results

420 3.1. Fabric analysis

421 The rose diagrams in Fig. 6 visualise the circular distributions of the examined
422 specimens. Overall, the UA4 sample and the sample of elephant bones show predom-
423 inant peaks in the NE quadrant; while the ones from units UA3c and UB4c suggest
424 multimodal distributions. Specifically, the UA4 sample distribution (Fig. 6b) spreads
425 largely in the NE quadrant. Similarly, the circular distribution of the elephant sam-
426 ple (Fig. 6c), mainly lying in UA4, resembles the former distribution: it is skewed to
427 the SW and concentrated in the NE quadrant. On the other hand, the UA3c sample
428 (Fig. 6a) shows a plurimodal distribution with two peaks to the E and NE, and the two
429 samples from Area B (Fig. 6d,e) suggest a different multimodal scenario.

430 Table 3 summarises the results of the circular uniformity tests. % UA3c – Mean
431 direction: 77.17° (E), circular variance: 41.95°; Mean dip: 20.35°, variance: 4.36°
432 With regard to the UA3c sample, the Rayleigh test (p – value = 0.029) rejected the null
433 hypothesis of circular uniformity. The mean resultant length ($\bar{R} = 0.268$) and the mean
434 direction of 77.17° are thus significant, assuming the distribution is unimodal. How-
435 ever, the rose diagram (Fig. 6a) shows a multimodal distribution. The Kuiper, Watson
436 and Rao omnibus tests, more powerful than the Rayleigh test in detecting multimodal

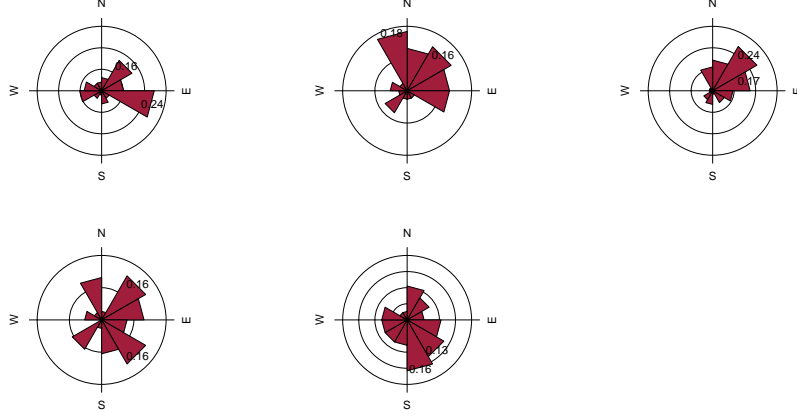


Figure 6: Rose diagrams showing the bearing patterns of samples from UA3c (a), UA4 (b), the elephant carcass (c) and UB4c (d: clock method, e: compass method).

437 deviation from uniformity, also rejected the null hypothesis of uniformity, therefore
438 suggesting significant multimodal anisotropy in the distribution.

439 For the UA4 sample and the subset of elephant bones, all the tests agreed in rejecting
440 the null hypothesis in favour of a preferentially oriented distribution. The Elephant
441 sample, with respect to the other, showed stronger anisotropy and significantly higher
442 \bar{R} . As suggested by the rose diagrams (Fig. 6c), this sample has a mean direction to-
443 wards the NE (55°) and relatively low circular variance (29°).

444 The UB4c sub-samples had discordant test results when considering the Rayleigh
445 and the omnibus statistics. According to the Rayleigh test, the mean resultant length
446 (\bar{R}) and the mean direction were not significant for the sub-sample of measurements
447 recorded with the clock system. However, this sample does not respect the assump-
448 tion of unimodality of the Rayleigh test (Fig. 6d). Conversely, a significant test result
449 was obtained for the sub-sample of measurements recorded using the compass, which
450 shows a normal (von Mises) distribution (Fig. 6e).

451 The results obtained for the UA3c sample and the UB4c sub-sample recorded using
452 the clock method are most probably due to the shape of those distributions. Indeed, the
453 clock system, being less accurate, tends to produce a less dense distribution, more
454 subject to show a multimodal shape when the distribution is actually uniform (Fig. 6a,
455 d).

456 The Woodcock eigenvalues ratio graph (Fig. 7a) presents the shape (K) and strength
457 (C) of the distributions. Fig. 7b plots confidence levels of Monte-Carlo critical C val-
458 ues, varying for sample sizes. The two samples from Area B, together with the UA3c
459 sample, having low C values, plotted close to the origin of the ratio graph. Thus,
460 they suggest weak preferential orientation (UA3c) and nearly significant randomness
461 (UB4c). On the other hand, the UA4 and the elephant samples, with higher C values,
462 showed a stronger and significant tendency to orient preferentially. The shape param-
463 eter K of the samples varied from $K = 0.2$ for the UB4c sample measured with the

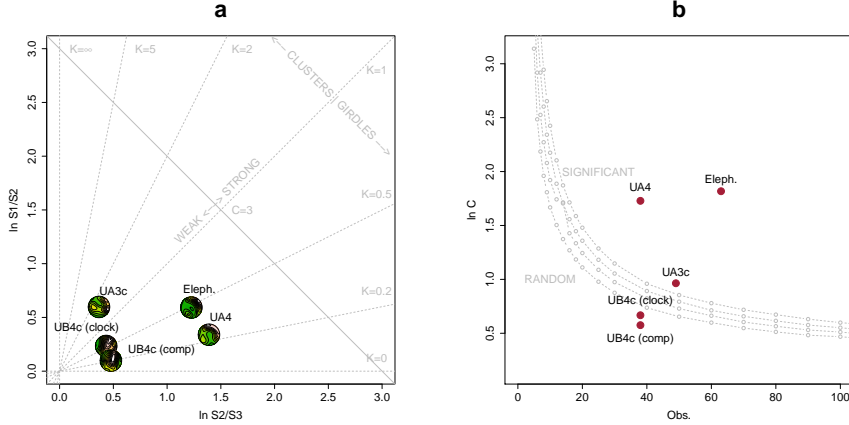


Figure 7: Woodcock's eigenvalues ratio graph (a) and plot of the Monte-Carlo critical S_1/S_3 test values, for varying sample sizes and confidence levels (b), modified from [Woodcock and Naylor \(1983\)](#).

compass, to $K = 0.6$ for the one measured with the clock, to $K = 5$ for the elephant sample. Overall, all the samples, except the UA3c one, plotted below the average shape value ($K = 1$) between girdles and clusters distributions.

The Benn diagram (Fig. 8) resembles the Woodcock ratio graph (Fig. 7a). The samples from units UB4c and UA3c clearly plotted at a distance from the UA4 and the elephant samples. The UB4c samples plotted in the upper corner of the ternary graph, with the UB4c sub-sample of measurements taken using the clock system exhibiting more isotropy. The UA3c sample, with an elongation index similar to the elephant sample, but higher isotropix index, plotted towards the centre.

Compared to the ranges recorded for modern natural processes (debris flow, runoff, solifluction), the fabric from the UA3c and UB4c units plotted well inside the cluster of debris flows, with the UB4c (clock) sample suggesting even more random orientations. On the other hand, the sample of elephant remains, which lie mostly on UA4 and are covered by UA3c, plotted significantly close to the sample from unit UA4. They both presented the lowest isotropy index (IS), but not high elongation index (EL). Thus, they plotted in the average between linear and planar orientations, within the range of runoff processes. Yet they still plotted at the margins of the cluster of debris flows fabrics. Moreover, the elephant sample showed a more linear attitude with respect to the UA4 sample.

3.2. Vertical distribution

Fig. 9 compares the distribution of the absolute elevations of the partial skeleton of the *Elephas (P.) antiquus* with the other remains from Area A. Overall, the vertical distribution of the elephant approximates a normal distribution with mean (μ) 349.25 m a.s.l. and standard deviation (σ) 0.12 m. The mean elevation of the erosional contact between the two stratigraphic units is slightly above the latter ($\mu = 349.30$ m). Al-

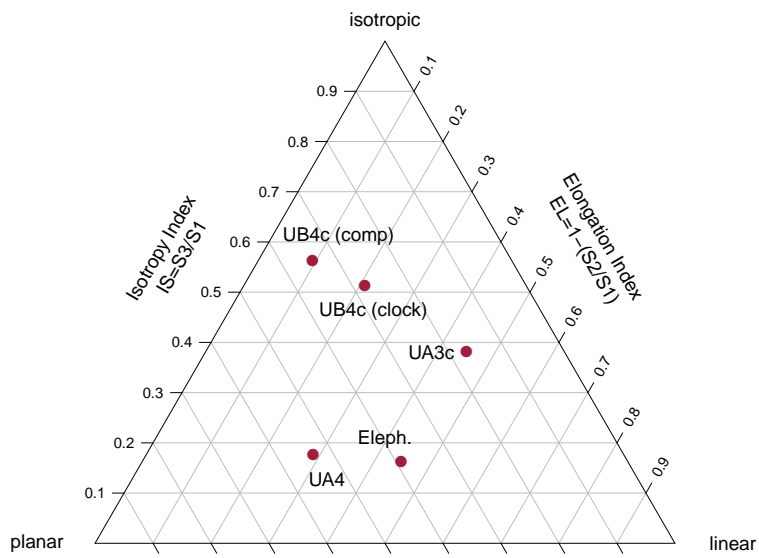


Figure 8: Benn's diagram. Fabric ranges of natural processes modified from Bertran et al. (1997); Lenoble and Bertran (2004).

489 though difficult to quantify due to its mixed nature, the range of elevations of this contact,
490 as estimated from the IDW interpolation (Fig. 9a), is relatively small ($\sigma = 0.06$ m).

491 Three lithic artefacts (two flakes and one tool) from the UA3c unit are located
492 within its positive half. Only one flake has been found in the lower UA4, at about
493 349.10 m, together with three chips. However, they plotted well within the left tail
494 of the debris/chip distribution from the unit above. Despite the scarcity of debitage
495 products in this area, waste products (debris/chip) are relatively well represented (16%
496 of the UA3c sample). Their vertical distribution approximates a normal distribution
497 ($\mu = 349.50$ m and $\sigma = 0.18$ m), having almost 50% of the sample in the range of
498 elevations of the erosional surface and the rest above it. Notably, the distribution of
499 the faunal remains from the same unit resembles that of the debris/chip. The Welch
500 two sample t-test ($p - value = 0.5099$) failed to reject the null hypothesis that the
501 two population means are equal. On the other hand, the vertical distribution of faunal
502 remains recovered from the UA4 unit is comparable with that of the *Elephas* ($p -$
503 $value = 0.6562$). Nevertheless, the density functions altogether clearly confirm one
504 of the main observations assessed during excavation, namely that the elephant remains
505 and most of the recovered faunal and lithic material in Area A lie at or close to the
506 UA3c/4 contact, with unit UA3c covering the remains.

507 Fig. 10 shows the empirical density functions of the minimum distances from each
508 specimen from Area B to the UB4c/5a erosional contact (Fig. 5b). The combined
509 distribution of any type of find from the UB5a unit (Fig. 10a) skewed to the left with
510 a short tail (up to -0.3 m). The mode, between 5 and 10 cm below the roof of UB5a,
511 indicates a general concentration of material very close to the contact of this unit with
512 the overlying UB4c, in accordance with the mean distribution of the different classes of
513 remains. Although the majority of both the lithic and faunal assemblages were found
514 in the uppermost 15 cm of UB5a, few debris/chips and bone fragments occur lower
515 in the sequence, yet no more than 30 cm below the roof of this unit. Very few flakes,
516 three tools and no cores have been found in this unit. As a whole, the lithic assemblage
517 from UB5a, mostly composed by debris/chips, is only 7% of the most conspicuous
518 assemblage from UB4c.

519 The global distribution of unit UB4c was right skewed (up to almost 0.6 m) and
520 centred at about 5 cm above the contact with the underlying unit UB5a (Fig. 10b).
521 Almost 30% of the sample fell exactly at the erosional contact that separates UB4c
522 from UB5a. The density estimations of the lithic debris/chip, flakes, tools and faunal
523 remains significantly overlap, whereas the distribution of the six cores shows a bimodal
524 shape with peaks at 5 and 20 cm above the contact. However, the Welch Two Sample t-
525 test of the lithic and faunal sample means failed to reject the null hypothesis ($p-value =$
526 0.6295).

527 3.3. Point pattern analysis

528 Results of the point pattern analysis are complementary to those obtained from the
529 analysis of the vertical and fabric distributions.

530 Regarding Area A, kernel density estimation and three-dimensional functions were
531 applied in order to quantitatively depict the spatial distribution of the lithic assemblage
532 in relation to the elephant skeleton.

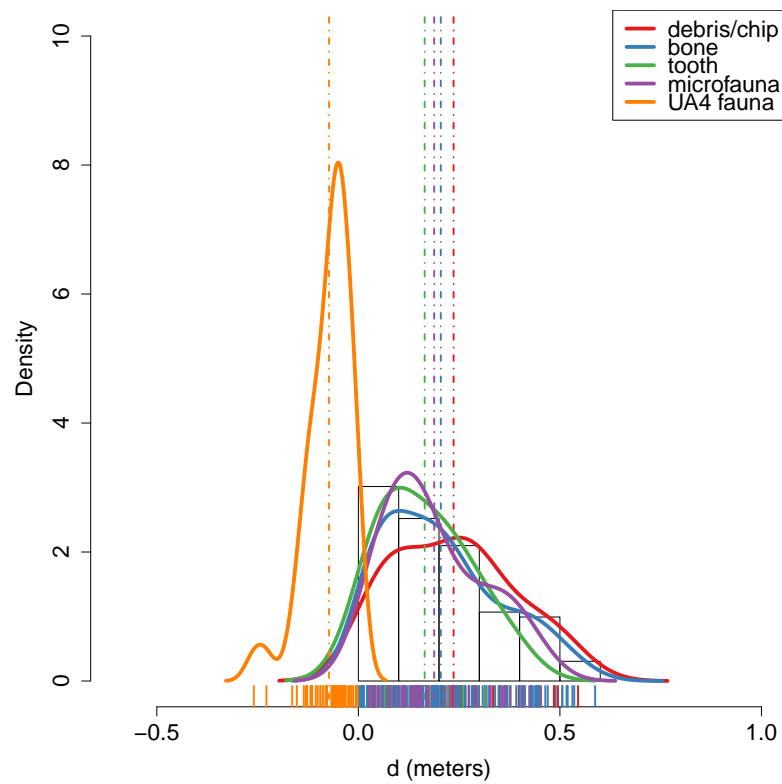


Figure 9: Empirical density functions of absolute elevations (meters a.s.l) of remains from Area A. The histogram represents the *Elephas (P.) antiquus* range of elevations; the grey area shades the $Q_3 - Q_1$ range of the erosional UA3c/4 surface; dashed lines indicate mean values.

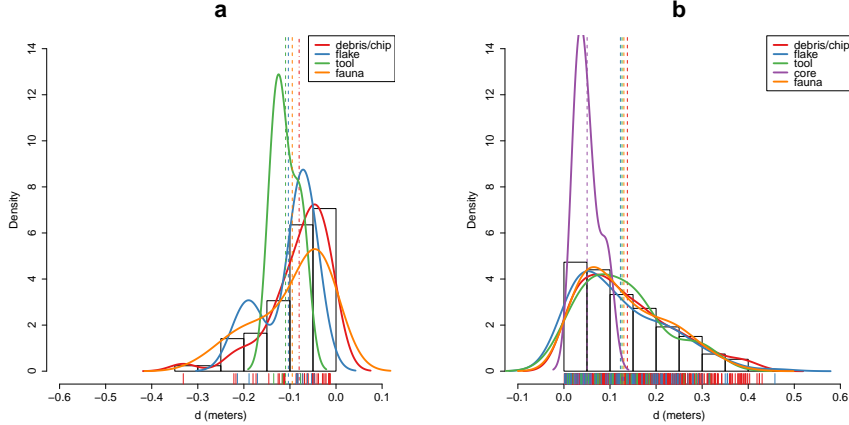


Figure 10: Empirical density functions of minimum orthogonal distances (d) to the UB4c/5a surface. The histogram represents the total distribution of remains from UB5a (a) and UB4c (b); dashed lines indicate mean values.

533 Fig. 11a shows the smoothing kernel intensity estimation of the faunal assemblage
 534 from the UA3c unit. Contour lines delimit the density of the lithic sample. The partial
 535 skeleton of the *E. (P.) antiquus* is superimposed on it. A preliminary visual examination
 536 of the plot suggests a homogeneous distribution of lithics (mostly debris/chips) and
 537 fossils. Spots of higher density appear to be spread around and in association with the
 538 elephant remains.

539 The univariate pair correlation function of the joined lithic assemblage from the
 540 UA3c and UA4 units (Fig. 11b) suggests aggregation of finds. The estimated $\hat{g}_3(r)$
 541 function (black solid line) wanders above the benchmark value (red dotted line) until
 542 values of $r = 0.8$. However, for distances between 35 and 65 cm, it lies above the
 543 grey envelope of significance for the null hypothesis of CSR, indicating that at those
 544 distances artefacts occur closer than expected in the case of random processes. For
 545 values of $r > 0.8$, the function stabilises at values close to 0, suggesting a Poisson
 546 distribution. The plot illustrates the random distribution of finds between patches of
 547 clusters that we observe in the kernel density estimation (Fig. 11a).

548 The histogram in Fig. 11c shows the density of the distances calculated from each
 549 artefact to the nearest-neighbour elephant remain. A right skewed distribution, with
 550 a prevalent peak at 10 cm and mean μ 30 cm is an indication of the relatively strong
 551 aggregation of events around the mass of the elephant skeleton.

552 As for Area B, the analysis first focused on the spatial distribution and cross-
 553 correlation of the assemblages from UB4c and UB5a (Fig. 12); and secondly on the
 554 interaction between classes of remains from UB4c (Fig. 13).

555 Figs. 12a,b respectively show kernel density estimations of the combined lithic and
 556 faunal assemblages from both the units analysed. Despite the samples size difference,
 557 a first visual examination suggests the presence of interesting spatial structures.

558 Regarding the UB4c unit (Fig. 12a), the high density of material concentrated

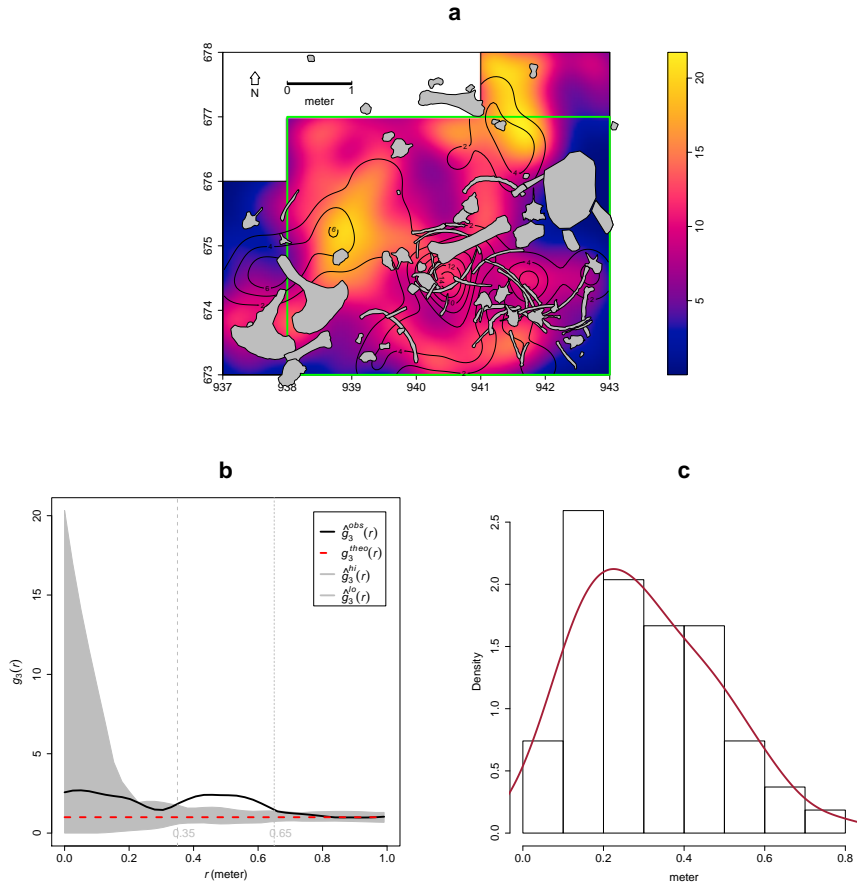


Figure 11: Kernel smoothed intensity function of the lithic and faunal assemblages from UA3c. Isolines mark the density of the lithic artefacts (a). Pair correlation function ($g_3(r)$) of a three-dimensional pattern of lithic artefacts from UA3c and UA4. Grey envelope of 999 Monte Carlo simulations under the CSR null hypothesis (b). Three-dimensional distance from each lithic artefact from UA3c and UA4 to the nearest neighbour elephant remain (c).

around the western square 934/600 suggests that the pattern could have been the result of an inhomogeneous, non-uniform depositional process. Visual comparison of the density plot with the elevation model of the erosional contact between the UB4c and UB5a units (Fig. 5b) suggests positive correlation between lower elevations (topographic depressions) and higher density of remains. Fig. 12c shows the results of the ρ -function, which estimates the intensity of the UB4c sample assemblage as a function of the covariate underlying topography created by the erosional event. Within the range of elevation between 350.2 and 350.4 m, the occurrence of finds is higher and the intensity decreases with the rise of elevation, i.e., finds are more likely to be found at lower elevations than would be expected if the intensity was constant.

Spatial Kolmogorov-Smirnov and Berman's Z_2 (Berman, 1986) statistics were used in order to test the dependence of the UB4c pattern on the covariate erosional surface. Both KS ($D = 0.11952$, $p - \text{value} = 7.772e - 16$) and Z_2 ($Z_2 = -7.8447$, $p - \text{value} = 4.34e - 15$) significantly rejected the null hypothesis of CSR. Although the tests suggested evidence that the intensity depends on the covariate, the effect of the covariate is weak and it seems to have no discriminatory power. The ROC curve and AUC statistics (0.56), which measure the strength of the covariate effect, suggest that the underlying UB4c/5a topography does not completely explain the localised high density of occurrence in the UB4c.

Relative spatial segregation seems to occur between the assemblages from UB4c (Fig. 12a) and UB5a (Fig. 12b), with high density of the former distribution corresponding to low density of the latter. The former analysis of the vertical distribution showed that the two assemblages occur very close to their stratigraphic contact. In order to further investigate the spatial interaction between the two depositional events, we applied multitype pair correlation ($g_{ij}(r)$) and nearest-neighbour ($G_{ij}(r)$) functions.

Fig. 12d shows the estimated values of the multivariate $\hat{g}_{ij}(r)$ function against the envelope of the null hypothesis, obtained by randomly shifting the position of remains from the two distributions in 199 Monte Carlo simulations. For fixed values of r less than 30 cm the observed function lies below the benchmark value of independence, thus indicating segregation; but it wanders at the lower edge of the grey envelope. For fixed distances of $r > 0.3$ m the observed and theoretical lines significantly overlap. Overall, the function suggests independence of the two point processes (UB4c and UB5a) at multiple scales.

However, the estimated $\hat{G}_{ij}(r)$ function (Fig. 12c), running well below the significance grey envelope for fixed values of $r > 0.3$ m, confirms that the nearest-neighbour distances between remains from UB4c and UB5a are significantly longer than expected in the case of independent processes. Interestingly, at values of $r < 0.2$ m the observed function failed to reject the null hypothesis of Complete Spatial Randomness and Independence (CSRI).

With the aim to integrate the vertical distribution analysis, the particle size spatial distribution of remains from the UB4c unit were investigated by means of a derivative of the multitype K -function, randomly labelling the classes of remains. Fig. 13 shows a selection of the array of possible combinations between classes. In any panel, the estimated function wanders above the benchmark value. Such positive deviations from the null hypotheses suggest that debris/chips are more likely to be found close to the other class of remains than would be expected in case of a completely random

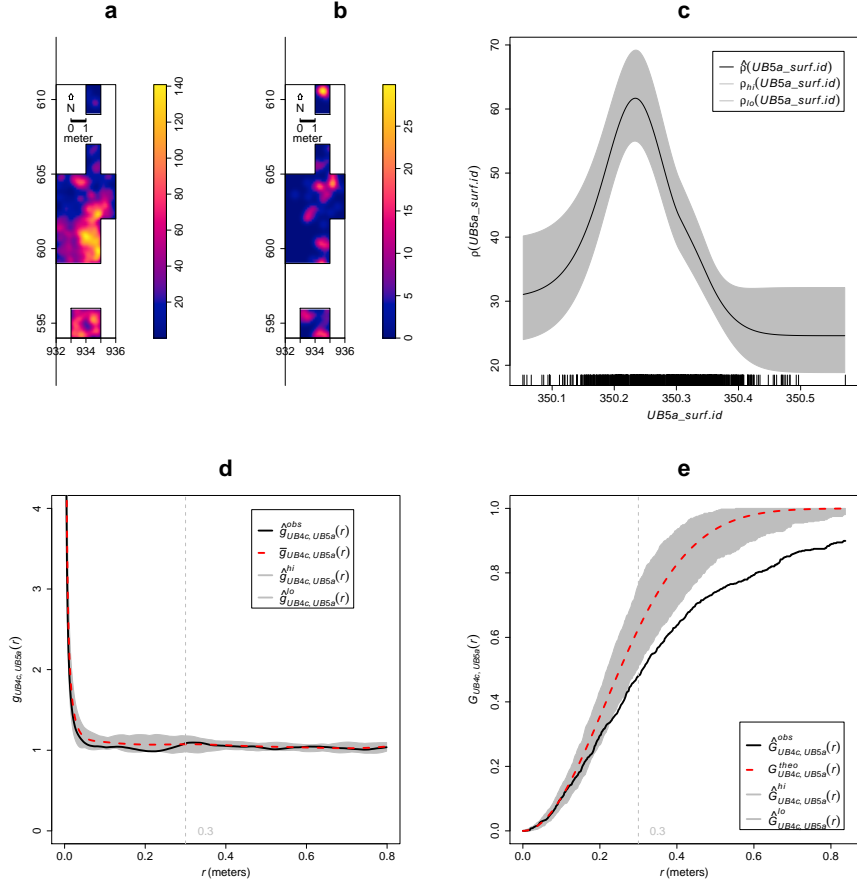


Figure 12: Kernel smoothed intensity function of the lithic and faunal assemblages from UB4c (a) and UB5a (b). Smoothing estimate of the intensity of remains from UB4c, as a function of the erosional surface UB4c/5a. Grey shading is pointwise 95% confidence bands (c). Cross-pattern pair correlation function ($g_{ij}(r)$) between the UB4c and UB5a distributions. Grey envelope of 199 Monte Carlo simulations under the independence of components null hypothesis (d). Multitype nearest-neighbour function ($G_{ij}(r)$) between the UB4c and UB5a distributions (e).

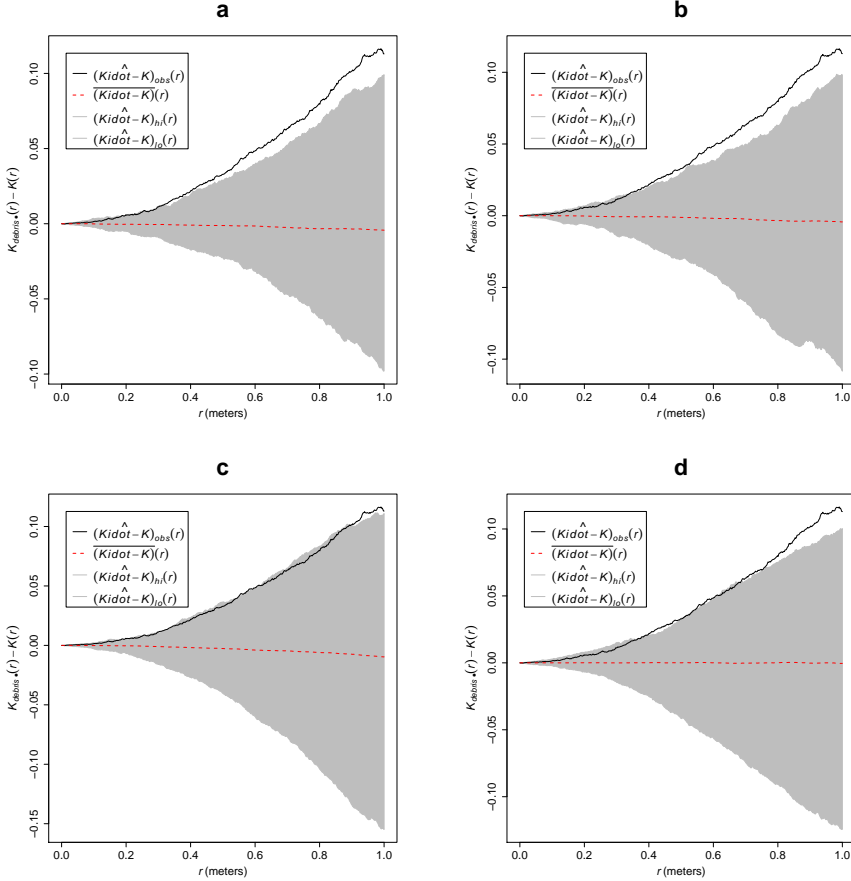


Figure 13: Random labelling test for the UB4c assemblage. Grey pointwise envelope of 199 Monte Carlo permutation of debris/chips with flakes (a); tools (b); cores (c); fossils (d).

605 distribution. Permutating the lithic debris/chips with flakes (Fig.13a), tools (Fig.13b),
 606 cores (Fig.13c) and faunal remains (Fig.13d), the Monte Carlo test results would have
 607 been significantly consistent with clustering, if we had chosen distance values $r > 0.4$,
 608 $r > 0.4$, $r > 0.9$, $r > 0.8$, respectively. Conversely, we could not reject the null
 609 hypothesis of CSRI for lesser values of r .

610 4. Discussion

611 Recent excavations at the Middle Pleistocene site of Marathousa 1 have unearthed
 612 in one of the two investigated areas (Area A) a partial skeleton of a single individual of
 613 *Elephas (P.) antiquus*, whose bones are in close anatomical association, and spatially
 614 and stratigraphically associated with lithic artefacts and other faunal remains. In Area
 615 B, 60 m to the South of Area A, we collected a much higher number of lithic artefacts

616 (Tourloukis et al., this issue), spatially and stratigraphically associated with other fau-
617 nal remains, including isolated elephant bones, cervids and carnivores among others
618 (Konidaris et al., this issue).

619 The two areas are stratigraphically correlated, the main fossiliferous layers (UA3c
620 and UB4c) representing a massive depositional process, such as a hyperconcentrated
621 flow that dumped material in a lake margin context (Karkanas et al., this issue).

622 To date, evidence of butchering (cut-marks) has been identified on two bones of
623 the elephant skeleton from Area A, as well on elephant and other mammal bones from
624 Area B (see Konidaris et al. (this issue)).

625 However, due to the secondary depositional nature of the main fossiliferous hori-
626 zon, it is of primary importance to evaluate the degree and reliability of the spatial
627 association of the lithic artefacts with the faunal remains, and especially with the ele-
628 phant skeleton. In order to tackle our main objective, we applied a comprehensive
629 set of spatial statistics to the distributions of the archaeological and zooarchaeologi-
630 cal/palaeontological remains from relevant stratigraphic units of the two areas of in-
631 vestigation. Preliminary results of our analyses are here discussed for both areas.

632 4.1. Fabric analysis

633 The analysis of the orientation (dip and strike) of subsets of remains, mostly bone
634 fragments, organic residues and lithic artefacts, showed different patterns for the two
635 main find-bearing units.

636 The test results (Tab. 3) for the UA4 sample and the sample of elephant remains
637 - which lie on unit UA4 and are covered by UA3c - indicated significant preferential
638 orientations towards the NE (Figs. 6b,c). As shown by the Woodcock's (Fig. 7) and the
639 Benn's diagrams (Fig. 8), these samples plotted together at a distance from the others.
640 Such convergence suggests that the elephant carcass, the other faunal remains and the
641 organic material, deposited on unit UA4, were subject to the same processes.

642 Far from the isotropic corner in the Benn's diagram these two samples from Area
643 A plotted approximately in between the linear and planar extremes, with the elephant
644 sample showing a more planar fabric. When the results published by Bertran et al.
645 (1997) and Lenoble and Bertran (2004) from observations of fabrics in modern sub-
646 aereal slope deposits were used as a reference, the two samples aggregated well within
647 the cluster of runoff process. Yet, they still plotted at the extreme margins of debris
648 flow and relatively distant from the linear corner.

649 This result is consistent with the exposure of unit UA4 to overland water-laden
650 processes that occurred before the flood event UA3/UB4 (Karkanas et al., this is-
651 sue). Notably, the erosive nature of low-energy processes triggered by rain-water has
652 been observed on lacustrine floodplains, and is associated with anisotropic patterns
653 in autochthonous assemblages (Cobo-Sánchez et al., 2014; Domínguez-Rodrigo et al.,
654 2014c; García-Moreno et al., 2016).

655 On the other hand, the fabric of the UA3c sample, being similar to those of the
656 UB4c sub-samples (Figs. 7 and 8), supports the stratigraphic correlation between these
657 units across the two investigated areas. The fabric analysis suggests that the UA3/UB4
658 process can be categorized as a flood event, which falls in between the spectrum of de-
659 bris and hyperconcentrated flow. Indeed, random distribution and orientation of clasts

660 is expected for debris flows, except at flow margins, where preferential orientation and
661 clusters of clasts have been observed (Pierson, 2005).

662 Unlike bones with a tubular shape (i.e., long bones), ribs and vertebrae are prone
663 to orient preferentially under high energy processes, less likely under low energy pro-
664 cesses (Domínguez-Rodrigo and García-Pérez, 2013; Domínguez-Rodrigo et al., 2014c).
665 Interestingly, whereas some of the ribs share the same preferential orientation with the
666 long bones, others are oriented NW/SE. However, a NW/SE orientation could be con-
667 sistent with a prevalent NE direction of the flow (and vice-versa), since long bones
668 could roll orthogonally to the flow direction (Voorhies, 1969).

669 On the other hand, a higher energy flood would lead to an under-representation
670 of most cancellous grease-bearing bones, which are prone to be easily transported by
671 water induced processes (Voorhies, 1969). Yet several carpals, tarsals, metapodials,
672 phalanges, ribs and vertebrae are present and in close spatial association with the ele-
673 phant cranium and other skeletal elements.

674 The presence of many of the skeletal elements suggests that the elephant carcass
675 was not subjected to high energy processes. Thus, we can assume that relatively low
676 energy overland flows slightly reworked and oriented the exposed elements of the
677 already dismembered (and probably already marginally displaced) elephant carcass,
678 which mostly preserves close anatomical associations, but not anatomical connections.

679 In Area B, two sub-samples from the same stratigraphic unit were analysed, accord-
680 ing to the different methods used for recording the orientation (dip and strike) of the
681 finds (i.e., 'clock' vs. compass), mostly faunal remains, wood fragments and lithic arte-
682 facts. Due to the different shapes of the two distributions (Figs. 6d,e), test statistics re-
683 ported contrasting results (Tab. 3). Indeed, the clock system, recording non-continuous
684 circular data, tends to produce a distribution more subject to show a multimodal shape
685 when the distribution is actually uniform. However, the three-dimensional Woodcock
686 (Fig. 7) and Benn (Fig. 8) diagrams agreed upon assessing the randomness of the sam-
687 ples. Despite minor differences between the two samples, both plotted with the UA3c
688 sample in the reference range of debris flows.

689 4.2. Vertical distribution

690 As for the vertical distribution, we assume that mass wasting processes, such as
691 debris or hyperconcentrated flows, would predominantly distribute extremely poorly
692 sorted clasts homogeneously throughout the sequence. Normal or inverse grading can
693 be observed in such flows (Pierson, 2005). A concentration of unsorted elements in the
694 proximity of the erosional surface, as well as the absence of any grading, would in turn
695 suggest an autochthonous assemblage.

696 The lithic assemblage from Area A - the combined sample from units UA3c and
697 UA4 ($n = 54$), composed by a fewdebitage products and a relatively high number of
698 debris/chips and retouch waste products (Tab. 2) - plotted predominantly in the prox-
699 imity of the erosional surface created by the UA3/UB4 event. The faunal remains
700 from unit UA3c resemble the distribution of the archaeological assemblage as a whole;
701 whereas the ones from the underlying unit UA4 match the vertical distribution of the
702 elephant (Fig. 9).

703 Overall, the material recovered from unit UA3c did not show any grading and
704 mainly plotted at the bottom of the unit, thus is consistent with the hypothesis of an
705 autochthonous assemblage.

706 In Area B, two samples from units UB4c ($n = 1243$) and UB5a ($n = 101$) respec-
707 tively, were analysed (Tab. 2) for quantifying the minimum orthogonal distance of each
708 item to the modelled erosional surface (Fig. 5b).

709 The vertical distribution of lithic artefacts and fossils from unit UB4c showed a pre-
710 dominant peak right at the contact with the erosional surface. Almost 30% of this rich
711 sample plotted at a distance between 0 and 5 cm from the erosional contact; whereas
712 the rest gently skewed to the upper part of the unit, up to about 50 cm. The same distri-
713 bution was observed for all classes of remains, suggesting no size sorting and an origin
714 very close to the erosional surface (Fig. 10b).

715 The density distribution of the sample from the underlying UB5a unit (Fig. 10a)
716 globally indicates a more constrained vertical displacement of remains (within 30 cm
717 below the erosional surface). Whereas lithic artefacts and fossils mostly plot right at
718 the contact and just below it, a few debris/chips and faunal remains were found lower
719 in the sequence. No size sorting was observed, but, notably, lithic cores are absent and
720 the debris/chip distribution is wider than the distribution of the few flakes and tools.

721 Field observations of cracks in the clayey UB5a unit testify to shrinking and swelling
722 during wet and dry cycles (Karkanas et al., *this issue*), which suggests that vertical dis-
723 placement of some small lithics and fossil fragments at lower depths with respect to
724 the UB5a/4c contact probably resulted from clay desiccation.

725 Likewise, Lenoble and Bertran (2004) documented up to 30 cm vertical dispersion
726 and frequent vertical dip of artefacts from the marshy silty clay of the Croix-de-Canard
727 site, sector 3.

728 Furthermore, a recent experimental study of animal trampling in water saturated
729 substrates reported negative correlation with artefact size, significant inclination and
730 greater vertical displacement than any former work: a maximum between 16 and
731 21 cm, with a mean of about 6 cm (Eren et al., 2010).

732 The fact that the majority of the remains from units UB4c and UB5a plotted at,
733 or very close to the contact between these two layers, the relatively high percentage
734 of lithics in both units, as well as the absence of size sorting or grading, suggest au-
735 tochthonous assemblages, deposited in UB5a and subsequently eroded *in situ* by the
736 UA3/UB4 flood event.

737 4.3. Point pattern analysis

738 The hypothesis that in both areas the lithic and faunal assemblages were primarily
739 deposited *in situ* and were subsequently reworked by a low energy flood, was further
740 explored by means of point pattern analysis.

741 We assumed that a completely random spatial distribution of the lithic artefacts
742 and faunal remains would suggest an allochthonous origin and subsequent transport to
743 the site by the action of a random massive process, such as debris flow. Nevertheless,
744 clustering of artefacts is not necessarily evidence of human presence. Aggregation or
745 segregation patterns could be produced by a range of biotic and/or natural processes.
746 Human activities, topography and physical obstructions alike could trigger spatial ag-
747 gregation.

748 The three-dimensional distribution of lithic artefacts from unit UA3c shows significant
749 clustering for values of r between 35 and 65 cm. Lithic artefacts occur relatively
750 close to the skeletal elements of the elephant, at a distance between 20 and 50 cm at
751 most (Fig. 11). The richest cluster of about 20 lithic artefacts is located to the SW of
752 the cranium, close to the right femur and the scatter of ribs and vertebrae.

753 Considering the prevalent NE orientation of the elephant bones and the other faunal
754 remains from UA4, it is not unlikely that a SW/NE oriented flood could have been
755 responsible for the observed accumulation to the SW of the elephant cranium, which
756 would have represented an important obstruction to the flow. A similar case of clus-
757 tering of small remains, apparently dammed by a long elephant tusk, has also been
758 observed at Castel di Guido (Italy) (Boschian and Saccà, 2010). Secondary deposi-
759 tion by low-energy flows and clustering of artefacts and bones blocked by an aurochs
760 carcass have been as well documented at the site of 'Ein Qashishadd (Israel) (Hovers
761 et al., 2014).

762 As mentioned above, whereas fairly random fabric and spatial distribution of coarse
763 clasts are observed at the centre of modern debris flow deposits, preferential orientation
764 and clustering may occur at the margin of the flood (Pierson, 2005). Yet the fabric
765 analysis of the UA3c sample shows a random distribution, which falls within the range
766 of debris flow (Fig. 8), and the pair correlation function (Fig. 9b) suggests significant
767 clustering of lithic artefacts at relatively small scale: a pattern less likely to be produced
768 by a large scale massive process such as a debris flow. Moreover, clusters of lithic
769 artefacts occur as well in areas with lower densities of elephant bones.

770 Small scale clustering; proximity to the elephant remains and the erosional surface;
771 absence of spatial size sorting and, on the contrary, the presence of a relatively high
772 number of lithic debris/chips associated with some flakes and tools; close anatomical
773 spatial association of the elephant skeletal elements, slightly displaced and preferen-
774 tially oriented: these lines of evidences support the hypothesis of an autochthonous
775 deposition, subject to localised minor reworking.

776 A similar pattern can be observed in Area B, where an initial set of spatial statistics
777 confirmed that the inhomogeneous density of remains from unit UB4c (Fig. 12a) is
778 not completely explained by the covariate effect of the underlying complex topography
779 created by the erosional event UA3/UB4 (Fig. 5b).

780 Thus, we explored the relative spatial interaction between the UB4c and the un-
781 derlying UB5a samples. We assumed that complete spatial randomness of the two
782 independent depositional processes would occur in case of an exogenous origin and
783 transportation of the UB4c assemblage. The hypothesis of an autochthonous original
784 deposition of the faunal and lithic assemblages on the UB5a unit, subsequently eroded
785 *in situ* by a relatively high energy flood (UB4c), was tested by cross-pattern spatial
786 correlation functions (Figs. 12d,e). Whereas the two samples are vertically adjacent to
787 the erosional surface (Fig. 10), on the horizontal plane they are both more segregated
788 than expected for a random distribution.

789 Moreover, for the UB4c sample, an unsorted particle size spatial distribution was
790 confirmed (Fig. 13). The occurrence in the same place of small and large classes of
791 remains suggests that post-depositional processes, such as water winnowing, have not
792 severely affected the assemblage. Hyperconcentrated flows would have dumped mate-
793 rial onto the lake margin. In this way, particles would have been frozen and deposited

794 *en masse*. Hence their non-sorted spatial distribution.

795 Conversely, the extraordinary preservation and number of mint to sharp, unsorted
796 lithic artefacts from the UB4c unit; their density, positively correlated to the topog-
797 raphy, and significantly segregated from the underlying distribution of remains; the
798 vertical proximity of both assemblages from UB4c and UB5a to the erosional surface;
799 as well as the random orientation pattern of the former, suggest that significant dis-
800 placement of materials due to the erosional event can be excluded.

801 The faunal and lithic assemblages from unit UB4c therefore most likely derived
802 from the local erosion of exposed mudflat areas (UB5a layer) and have been slightly
803 redistributed by the same flood event that capped the elephant in Area A.

804 Further evidence that the recovered assemblage has not undergone substantial re-
805 working and has retained its original characteristics would come from the refitting anal-
806 ysis, currently in progress. To date, 4 bone refits have been found in Area B: three from
807 unit UB4c, respectively at 4.77, 0.05 and 0.01 m distance; and one between two mam-
808 mal bone fragments from units UB4c and UB5a, at a very short distance (0.09 m).
809 Interestingly, one of the elements of the most distant refit (a *Dama sp.* mandibular
810 fragment) shows traces of carnivore gnawing ([Konidaris et al., this issue](#)).

811 In conclusion, multiple lines of evidence suggest that the erosional event UB4/UA3
812 represents a relatively low-energy process in the continuum between debris and hyper-
813 concentrated flow, which would have locally reworked at a small scale the already
814 exposed or slightly buried and spatially associated lithic and faunal assemblages.

815 Although the UB4/UA3 process represents a snapshot of a relatively short time-
816 frame, inferences about the use of space by human groups, in terms of knapping
817 episodes and butchering activities, are unreliable in light of the current information.

818 The spatial pattern observed at the site is indeed the result of the last episode in
819 a palimpsest of spatial processes. Whereas the erosional event represented by the de-
820 bris/hyperconcentrated flow UA3/UB4 caps the sequence and preserves the record, lit-
821 tle is known about the eroded underlying occupational horizon.

822 However, whereas hunting or scavenging is still an unsolved matter of debate, con-
823 sidering the rate of bone fragmentation, the density of lithic debris/chips, the number
824 of processed bones and their spatial density and association, it is likely that the assem-
825 blage represents a complex palimpsest of locally repeated events of hunting/scavenging
826 and exploitation of lake shore resources.

827 More data from high resolution excavations in the coming years will allow us to
828 refine the coarse-grained spatio-temporal resolution of our inferences about past human
829 behaviour at Marathousa 1.

830 5. Conclusions

831 At the Middle Pleistocene open-air site of Marathousa 1, a partial skeleton of a
832 single individual of *Elephas (Palaeoloxodon) antiquus* was recovered in stratigraphic
833 association with a rich and consistent lithic assemblage and other vertebrate remains.
834 Cut-marks and percussion marks have been identified on the elephant and other mam-
835 mal bones excavated at the site. The main find-bearing horizon represents a secondary
836 depositional process in a lake margin context.

837 Understanding the site formation processes is of primary importance in order to
838 reliably infer hominin exploitation of the elephant carcass and other animals. To meet
839 this aim, we applied a comprehensive set of multivariate and multiscale spatial analyses
840 in a taphonomic framework.

841 Results from the fabric, vertical distribution and point pattern analyses are consis-
842 tent with a relatively low-energy erosional process slightly reworking at a small scale
843 an exposed (or slightly buried) and consistent scatter of lithic artefacts and faunal re-
844 mains. These results are in agreement with preliminary taphonomic observations of the
845 lithic artefacts (Tourloukis et al., this issue) and the faunal remains (Konidaris et al.,
846 this issue), which also indicate minor weathering and transportation. Our analyses
847 show that multiple lines of evidence support an autochthonous origin of the lithic and
848 faunal assemblages, subject to minor post-depositional reworking. Human activities
849 therefore took place on-site, during an as of yet uncertain range of time.

850 **Acknowledgements**

851 This research is supported by the European Research Council (ERC StG PaGE
852 283503) awarded to K. Harvati. We are grateful to the Municipality of Megalopolis,
853 the authorities of the Region of Peloponnese, and the Greek Public Power corporation
854 (Δ EH) for their support. We also thank Julian Bega and all the participants in the PaGE
855 survey and excavation campaigns in Megalopolis for their indispensable cooperation.

856 **References**

- 857 Anderson, K. L., Burke, A., 2008. Refining the definition of cultural levels at Karabi
858 Tamchin: a quantitative approach to vertical intra-site spatial analysis. Journal of
859 Archaeological Science 35 (8), 2274–2285.
- 860 Aramendi, J., Uribelarrea, D., Arriaza, M. C., Arráiz, H., Barboni, D., Yravedra, J.,
861 Ortega, M. C., Gidna, A., Mabulla, A., Baquedano, E., Domínguez-Rodrigo, M.,
862 2017. The paleoecology and taphonomy of {AMK} (bed i, olduvai gorge) and its
863 contributions to the understanding of the “zinj” paleolandscape. Palaeogeography,
864 Palaeoclimatology, Palaeoecology, –.
865 URL [http://www.sciencedirect.com/science/article/pii/
866 S0031018216308112](http://www.sciencedirect.com/science/article/pii/S0031018216308112)
- 867 Baddeley, A., Chang, Y.-M., Song, Y., Turner, R., 2012. Nonparametric estimation of
868 the dependence of a point process on spatial covariates. Statistics and Its Interface
869 5 (2), 221–236.
- 870 Baddeley, A., Rubak, E., Turner, R., 2015. Spatial Point Patterns: Methodology and
871 Applications with R. Chapman and Hall/CRC, London.
- 872 Bailey, G., 2007. Time perspectives, palimpsests and the archaeology of time. Journal
873 of Anthropological Archaeology 26 (2), 198 – 223.
874 URL [http://www.sciencedirect.com/science/article/pii/
875 S0278416506000481](http://www.sciencedirect.com/science/article/pii/S0278416506000481)

- 876 Bar-Yosef, O., Tchernov, E., 1972. On the palaeo-ecological history of the site of Ubeidiya. Vol. 35. Israel Academy of Sciences and Humanities, Jerusalem.
- 877
- 878 Bargalló, A., Gabucio, M. J., Rivals, F., 2016. Puzzling out a palimpsest: Testing
879 an interdisciplinary study in level o of abric romaní. Quaternary International
880 417 (Supplement C), 51 – 65, advances in Palimpsest Dissection.
- 881 URL [http://www.sciencedirect.com/science/article/pii/
882 S1040618215009635](http://www.sciencedirect.com/science/article/pii/S1040618215009635)
- 883 Benito-Calvo, A., de la Torre, I., 2011. Analysis of orientation patterns in Olduvai
884 Bed I assemblages using GIS techniques: Implications for site formation processes.
885 Journal of Human Evolution 61 (1), 50 – 60.
- 886 Benito-Calvo, A., Martínez-Moreno, J., Mora, R., Roy, M., Roda, X., 2011. Trampling
887 experiments at Cova Gran de Santa Linya, Pre-Pyrenees, Spain: their relevance for
888 archaeological fabrics of the Upper–Middle Paleolithic assemblages. Journal of Archaeological Science 38 (12), 3652–3661.
- 889
- 890 Benito-Calvo, A., Martínez-Moreno, J., Pardo, J. F. J., de la Torre, I., Torcal, R. M.,
891 2009. Sedimentological and archaeological fabrics in Palaeolithic levels of the
892 South-Eastern Pyrenees: Cova Gran and Roca dels Bous Sites (Lleida, Spain). Journal
893 of Archaeological Science 36 (11), 2566 – 2577.
- 894 Benn, D., 1994. Fabric shape and the interpretation of sedimentary fabric data. Journal
895 of Sedimentary Research 64 (4a), 910–915.
- 896 Benvenuti, M., Martini, I. P., 2002. Analysis of terrestrial hyperconcentrated flows and
897 their deposit. In: Martini, I. P., Baker, V. R., Garzón, G. (Eds.), Flood and Megaflood
898 Processes and Deposits. Vol. 32 of Special Publication of the International Association
899 of Sedimentologists. Blackwell Publishing Ltd., pp. 167–193.
- 900 URL <http://dx.doi.org/10.1002/9781444304299.ch10>
- 901 Berman, M., 1986. Testing for spatial association between a point process and another
902 stochastic process. Applied Statistics 35, 54–62.
- 903 Bernatchez, J. A., 2010. Taphonomic implications of orientation of plotted finds from
904 Pinnacle Point 13B (Mossel Bay, Western Cape Province, South Africa). Journal of
905 Human Evolution 59 (3–4), 274 – 288.
- 906 Bertran, P., Hetù, B., Texier, J.-P., Steijn, H. V., 1997. Fabric characteristics of subaerial
907 slope deposits. Sedimentology 44 (1), 1 – 16.
- 908 Bertran, P., Texier, J.-P., 1995. Fabric Analysis: Application to Paleolithic Sites. Journal
909 of Archaeological Science 22 (4), 521 – 535.
- 910 Bevan, A., Crema, E., Li, X., Palmisano, A., 2013. Intensities, Interactions, and Un-
911 certainties: Some New Approaches to Archaeological Distributions. In: Bevan, A.,
912 Lake, M. (Eds.), Computational Approaches to Archaeological Spaces. Left Coast
913 Press, Walnut Creek, pp. 27–52.

- 914 Binford, L. R., 1981. Behavioral archaeology and the "pompeii premise". Journal of
915 Anthropological Research 37 (3), 195–208.
- 916 Boschian, G., Saccà, D., 2010. Ambiguities in human and elephant interactions? Sto-
917 ries of bones, sand and water from Castel di Guido (Italy). Quaternary International
918 214 (1–2), 3 – 16.
- 919 Brantingham, P. J., Surovell, T. A., Waguespack, N. M., 2007. Modeling post-
920 depositional mixing of archaeological deposits. Journal of Anthropological
921 Archaeology 26 (4), 517 – 540.
922 URL [http://www.sciencedirect.com/science/article/pii/
923 S0278416507000359](http://www.sciencedirect.com/science/article/pii/S0278416507000359)
- 924 Carrer, F., 2015. Interpreting Intra-site Spatial Patterns in Seasonal Contexts: an Eth-
925 noarchaeological Case Study from the Western Alps. Journal of Archaeological
926 Method and Theory, 1–25.
- 927 Cobo-Sánchez, L., Aramendi, J., Domínguez-Rodrigo, M., 2014. Orientation patterns
928 of wildebeest bones on the lake Masek floodplain (Serengeti, Tanzania) and their
929 relevance to interpret anisotropy in the Olduvai lacustrine floodplain. Quaternary
930 International 322–323 (0), 277 – 284.
- 931 de la Torre, I., Benito-Calvo, A., 2013. Application of GIS methods to retrieve ori-
932 entation patterns from imagery; a case study from Beds I and II, Olduvai Gorge
933 (Tanzania). Journal of Archaeological Science 40 (5), 2446–2457.
- 934 Dibble, H. L., Chase, P. G., McPherron, S. P., Tuffreau, A., Oct. 1997. Testing the
935 reality of a "living floor" with archaeological data. American Antiquity 62 (4), 629–
936 651.
937 URL <http://www.jstor.org/stable/281882>
- 938 Diggle, P., 1985. A kernel method for smoothing point process data. Applied Statistics
939 (Journal of the Royal Statistical Society, Series C) 34, 138–147.
- 940 Domínguez-Rodrigo, M., Bunn, H., Mabulla, A., Baquedano, E., Uribelarrea, D.,
941 Pérez-González, A., Gidna, A., Yravedra, J., Diez-Martin, F., Egeland, C., Barba,
942 R., Arriaza, M., Organista, E., Ansón, M., 2014a. On meat eating and human evolu-
943 tion: A taphonomic analysis of BK4b (Upper Bed II, Olduvai Gorge, Tanzania), and
944 its bearing on hominin megafaunal consumption. Quaternary International 322–323,
945 129–152.
- 946 Domínguez-Rodrigo, M., Bunn, H., Pickering, T., Mabulla, A., Musiba, C., Baque-
947 dano, E., Ashley, G., Diez-Martin, F., Santonja, M., Uribelarrea, D., Barba, R.,
948 Yravedra, J., Barboni, D., Arriaza, C., Gidna, A., 2012. Autochthony and orientation
949 patterns in Olduvai Bed I: a re-examination of the status of post-depositional biasing
950 of archaeological assemblages from FLK North (FLKN). Journal of Archaeological
951 Science 39 (7), 2116 – 2127.

- 952 Domínguez-Rodrigo, M., Cobo-Sánchez, L., Yravedra, J., Uribelarrea, D., Arriaza, C.,
953 Organista, E., Baquedano, E., 2017. Fluvial spatial taphonomy: a new method for the
954 study of post-depositional processes. *Archaeological and Anthropological Sciences*,
955 1–21.
- 956 Domínguez-Rodrigo, M., Diez-Martín, F., Yravedra, J., Barba, R., Mabulla, A., Baque-
957 dano, E., Uribelarrea, D., Sánchez, P., Eren, M. I., 2014b. Study of the SHK Main
958 Site faunal assemblage, Olduvai Gorge, Tanzania: Implications for Bed II tapho-
959 nomy, paleoecology, and hominin utilization of megafauna. *Quaternary International*
960 322–323, 153–166.
- 961 Domínguez-Rodrigo, M., García-Pérez, A., 07 2013. Testing the Accuracy of Different
962 A-Axis Types for Measuring the Orientation of Bones in the Archaeological and
963 Paleontological Record. *PLoS ONE* 8 (7), e68955.
- 964 Domínguez-Rodrigo, M., Uribelarrea, D., Santonja, M., Bunn, H., García-Pérez, A.,
965 Pérez-González, A., Panera, J., Rubio-Jara, S., Mabulla, A., Baquedano, E., Yrave-
966 dra, J., Diez-Martín, F., 2014c. Autochthonous anisotropy of archaeological mate-
967 rials by the action of water: experimental and archaeological reassessment of the
968 orientation patterns at the Olduvai sites . *Journal of Archaeological Science* 41 (0),
969 44 – 68.
- 970 Eberth, D. A., Rogers, R. R., Fiorillo, A. R., 2007. A practical approach to the study of
971 bonebeds. In: Rogers, R. R., Eberth, D. A., Fiorillo, A. R. (Eds.), *Bonebeds. Genesis,*
972 *Analysis, and Paleobiological Significance*. The University of Chicago Press, pp.
973 265–332.
- 974 Enloe, J. G., 2006. Geological processes and site structure: assessing integrity at a late
975 paleolithic open-air site in northern france. *Geoarchaeology* 21 (6), 523–540.
- 976 Eren, M. I., Durant, A., Neudorf, C., Haslam, M., Shipton, C., Bora, J., Korisetar,
977 R., Petraglia, M., 2010. Experimental examination of animal trampling effects on
978 artifact movement in dry and water saturated substrates: a test case from South India.
979 *Journal of Archaeological Science* 37 (12), 3010 – 3021.
- 980 Fernández-López, S. R., 1991. Taphonomic concepts for a theoretical biochronology.
981 *Revista Española de Paleontología* 6, 37–49.
- 982 Fiorillo, A. R., 1991. Taphonomy and depositional setting of careless creek quarry
983 (judith river formation), wheatland county, montana, u.s.a. *Palaeogeography,*
984 *Palaeoclimatology, Palaeoecology* 81 (3), 281–311.
985 URL <http://www.sciencedirect.com/science/article/pii/003101829190151G>
- 987 García-Moreno, A., Smith, G. M., Kindler, L., Pop, E., Roebroeks, W., Gaudzinski-
988 Windheuser, S., Klinkenberg, V., 2016. Evaluating the incidence of hydrological
989 processes during site formation through orientation analysis. A case study of the
990 middle Palaeolithic Lakeland site of Neumark-Nord 2 (Germany). *Journal of Ar-
991 chaeological Science: Reports* 6, 82 – 93.

- 992 Giusti, D., Arzarello, M., 2016. The need for a taphonomic perspective in spatial analy-
993 sis: Formation processes at the Early Pleistocene site of Pirro Nord (P13), Apricena,
994 Italy. *Journal of Archaeological Science: Reports* 8, 235 – 249.
- 995 Harvati, K., Panagopoulou, E., Tourloukis, V., Thompson, N., Karkanas, P., Athanasi-
996 siou, A., Konidaris, G., Tsartsidou, G., Giusti, D., 2016. New Middle Pleistocene
997 elephant butchering site from Greece. In: Paleoanthropology Society Meeting. At-
998 lanta, Georgia, pp. A14–A15.
- 999 Hivernel, F., Hodder, I., 1984. Analysis of artifact distribution at Ngenym (Kenya):
1000 depositional and postdepositional effects. In: Hietala, H., Larson, P. (Eds.), *Intrasite*
1001 *Spatial Analysis in Archaeology*. Cambridge University Press, Ch. 7, pp. 97–115.
- 1002 Hodder, I., Orton, C., 1976. *Spatial Analysis in Archaeology. New Studies in Archae-*
1003 *ology*. Cambridge University Press, Cambridge.
- 1004 Hovers, E., Ekshtain, R., Greenbaum, N., Malinsky-Buller, A., Nir, N., Yeshurun,
1005 R., 2014. Islands in a stream? Reconstructing site formation processes in the late
1006 Middle Paleolithic site of 'Ein Qashish, northern Israel. *Quaternary International*
1007 331, 216–233.
1008 URL [http://www.sciencedirect.com/science/article/pii/
1009 S1040618214000433](http://www.sciencedirect.com/science/article/pii/S1040618214000433)
- 1010 Isaac, G. L., 1967. Towards the interpretation of occupation debris: Some experiments
1011 and observations. *Kroeber Anthropological Society Papers* 37 (37), 31–57.
- 1012 Jammalamadaka, S., Sengupta, A., Sengupta, A., 2001. *Topics in Circular Statistics.*
1013 Series on multivariate analysis
- 1014 World Scientific.
- 1015 Karkanas, P., Tourloukis, V., Thompson, N., Giusti, D., Panagopoulou, E., Harvati, K.,
1016 this issue. Sedimentology and micromorphology of the lower palaeolithic lakeshore
1017 site marathousa 1, megalopolis basin, greece. *Quaternary International*.
- 1018 Kluskens, S. L., 1990. Orientation and density analysis of stone artefacts at combe-
1019 capelle bas, périgord, france. Master's thesis, University of Pennsylvania.
- 1020 Konidaris, G., Athanassiou, A., Tourloukis, V., Thompson, N., Giusti, D.,
1021 Panagopoulou, E., Harvati, K., this issue. The elephas (palaeoloxodon) antiquus
1022 skeleton and other large mammals from the lower palaeolithic locality marathousa-
1023 1 (megalopolis basin, greece): preliminary results on taxonomy, biochronology,
1024 palaeoecology and taphonomy. *Quaternary International*.
- 1025 Krumbein, W. C., 1941. Measurement and geological significance of shape and
1026 roundness of sedimentary particles. *JOURNAL OF SEDIMENTARY PETROLOGY*
1027 11 (2), 64–72.
- 1028 Lenoble, A., Bertran, P., 2004. Fabric of Palaeolithic levels: methods and implications
for site formation processes. *Journal of Archaeological Science* 31 (4), 457 – 469.

- 1029 Lenoble, A., Bertran, P., Lacrampe, F., 2008. Solifluction-induced modifications
1030 of archaeological levels: simulation based on experimental data from a modern
1031 periglacial slope and application to French Palaeolithic sites. *Journal of Archaeo-*
1032 *logical Science* 35 (1), 99 – 110.
- 1033 Lindsay, J. F., 1968. The development of clast fabric in mudflows. *Journal of Sedimen-*
1034 *tary Research* 38 (4), 1242–1253.
1035 URL <http://jsedres.geoscienceworld.org/content/38/4/1242>
- 1036 Macdonald, D. I. M., Jefferson, T. H., 1985. Orientation studies of waterlogged wood;
1037 a paleocurrent indicator? *Journal of Sedimentary Research* 55 (2), 235–239.
1038 URL <http://jsedres.geoscienceworld.org/content/55/2/235>
- 1039 Malinsky-Buller, A., Hovers, E., Marder, O., 2011. Making time: ‘Living floors’,
1040 ‘palimpsests’ and site formation processes – A perspective from the open-air Lower
1041 Paleolithic site of Revadim Quarry, Israel. *Journal of Anthropological Archaeology*
1042 30 (2), 89 – 101.
1043 URL [http://www.sciencedirect.com/science/article/pii/
1044 S0278416510000632](http://www.sciencedirect.com/science/article/pii/S0278416510000632)
- 1045 Marwick, B., 2017. Computational reproducibility in archaeological research: Ba-
1046 sis principles and a case study of their implementation. *Journal of Archaeological*
1047 *Method and Theory* 24 (2), 424–450.
- 1048 Marwick, B., d’Alpoim Guedes, J., Barton, C. M., Bates, L. A., Baxter, M., Beavan,
1049 A., Bollwerk, E. A., Bocinsky, R. K., Brughams, T., Carter, A. K., Conrad, C.,
1050 Contreras, D. A., Costa, S., Crema, E. R., Daggett, A., Davies, B., Drake, B. L.,
1051 Dye, T. S., France, P., Fullager, R., Giusti, D., Graham, S., Harris, M. D., Hawks, J.,
1052 Heath, S., Huffer, D., Kansa, E. C., Kansa, S. W., Madsen, M. E., Melcher, J., Negre,
1053 J., Neiman, F. D., Opitz, R., Orton, D. C., Przystupa, P., Raviele, M., Riel-Salvatore,
1054 J., Riris, P., Romanowska, I., Smith, J., Strupler, N., Ullah, I. I., Vlack, H. G. V.,
1055 VanValkenberg, N., Watrall, E. C., Webster, C., Wells, J., Winters, J., Wren, C. D.,
1056 2017. Open science in archaeology. *SAA Archaeological Record* 17 (4), 8–14.
1057 URL <http://bit.ly/OSIG-SAAAR>
- 1058 McPherron, S. J., 2005. Artifact orientations and site formation processes from total
1059 station proveniences. *Journal of Archaeological Science* 32 (7), 1003 – 1014.
- 1060 McPherron, S. J., Dibble, H. L., Goldberg, P., 2005. Z. *Geoarchaeology* 20 (3), 243–
1061 262.
1062 URL <http://dx.doi.org/10.1002/gea.20048>
- 1063 Morton, A. G. T., 2004. Archaeological Site Formation: Understanding Lake Margin
1064 Contexts. No. 1211 in BAR International Series. Archaeopress, Oxford.
- 1065 Nickel, B., Riegel, W., Schonherr, T., Velitzelos, E., 1996. Environments of coal forma-
1066 tion in the Pleistocene lignite at Megalopolis, Peloponnesus (Greece) - reconstruc-
1067 tion from palynological and petrological investigations. *N. Jb. Geol. Palaont. A.* 200,
1068 201–220.

- 1069 Ohser, J., 1983. On estimators for the reduced second moment measure of point pro-
1070 cesses. *Mathematische Operationsforschung und Statistik, series Statistics* 14, 63–
1071 71.
- 1072 Organista, E., Domínguez-Rodrigo, M., Yravedra, J., Uribelarrea, D., Arriaza, M. C.,
1073 Ortega, M. C., Mabulla, A., Gidna, A., Baquedano, E., 2017. Biotic and abiotic pro-
1074 cesses affecting the formation of BK Level 4c (Bed II, Olduvai Gorge) and their bear-
1075 ing on hominin behavior at the site. *Palaeogeography, Palaeoclimatology, Palaeo-
1076 ecology*, –.
- 1077 Orton, C., 1982. Stochastic process and archaeological mechanism in spatial analysis.
1078 *Journal of Archaeological Science* 9 (1), 1 – 23.
- 1079 Panagopoulou, E., Tourloukis, V., Thompson, N., Athanassiou, A., Tsartsidou, G.,
1080 Konidaris, G., Giusti, D., Karkanas, P., Harvati, K., 2015. Marathousa 1: a new Mid-
1081 dle Pleistocene archaeological site from Greece. *Antiquity Project Gallery* 89 (343).
- 1082 Petraglia, M. D., Nash, D. T., 1987. The impact of fluvial processes on experimen-
1083 tal sites. In: Nash, D. T., Petraglia, M. D. (Eds.), *Natural formation processes and*
1084 *the archaeological record*. Vol. 352 of International Series. British Archaeological
1085 Reports, Oxford, pp. 108–130.
- 1086 Petraglia, M. D., Potts, R., 1994. Water Flow and the Formation of Early Pleistocene
1087 Artifact Sites in Olduvai Gorge, Tanzania . *Journal of Anthropological Archaeology*
1088 13 (3), 228 – 254.
- 1089 Pierson, T. C., 2005. Distinguishing between debris flows and floods from field evi-
1090 dence in small watersheds. Usgs numbered series, U.S. Geological Survey.
- 1091 R Core Team, 2016. R: A Language and Environment for Statistical Computing. R
1092 Foundation for Statistical Computing, Vienna, Austria.
- 1093 Ripley, B., 1977. Modelling spatial patterns. *Journal of the Royal Statistical Society, series B* 39, 172–212.
- 1095 Ripley, B., 1988. Statistical inference for spatial processes. Cambridge University
1096 Press.
- 1097 Ripley, B. D., 1976. The second-order analysis of stationary point processes. *Journal of Applied Probability* 13 (2), 255–266.
- 1099 Ripley, B. D., 1981. Spatial Statistics. John Wiley and Sons, New York.
- 1100 Schick, K. D., 1984. Processes of paleolithic site formation: an experimental study.
1101 Ph.D. thesis, University of California, Berkeley.
- 1102 Schick, K. D., 1986. Stone Age sites in the making: experiments in the formation
1103 and transformation of archaeological occurrences. Vol. 319 of International Series.
1104 British Archaeological Reports, Oxford.

- 1105 Schick, K. D., 1987. Modeling the formation of Early Stone Age artifact concentrations. *Journal of Human Evolution* 16, 789–807.
- 1107 Schiffer, M. B., 1972. Archaeological Context and Systemic Context. *American Antiquity* 37 (2), 156–165.
- 1109 Schiffer, M. B., 1983. Toward the identification of formation processes. *American Antiquity* 48 (4), 675–706.
- 1111 Schiffer, M. B., 1987. Formation processes of the archaeological record. University of New Mexico Press, Albuquerque.
- 1113 Shackley, M. L., 1978. The behaviour of artefacts as sedimentary particles in a fluvial environment. *Archaeometry* 20 (1), 55–61.
- 1115 Sánchez-Romero, L., Benito-Calvo, A., Pérez-González, A., Santonja, M., 12 2016. Assessment of Accumulation Processes at the Middle Pleistocene Site of Ambrona (Soria, Spain). Density and Orientation Patterns in Spatial Datasets Derived from Excavations Conducted from the 1960s to the Present. *PLOS ONE* 11 (12), 1–27.
- 1119 Texier, J.-P., 2000. A propos des processus de formation des sites préhistoriques / About prehistoric site formation processes. *Paléo* 12 (1), 379–386.
1121 URL http://www.persee.fr/web/revues/home/prescript/article/pal_1145-3370_2000_num_12_1_1610
- 1123 Toots, H., 1965. Orientation and distribution of fossils as environmental indicators. In: Nineteenth Field Conference of the Wyoming Geological Association. pp. 219–292.
- 1125 Tourloukis, V., Thompson, N., Panagopoulou, E., Giusti, D., Konidaris, G., Karkanas, P., Harvati, K., this issue. Lithic and osseous artifacts from the lower palaeolithic site of marathousa 1, megalopolis, greece: preliminary results. *Quaternary International*.
- 1128 van Vugt, N., de Bruijn, H., van Kolfschoten, M., Langereis, C. G., 2000. Magneto- and cyclostratigraphy and mammal-fauna's of the Pleistocene lacustrine Megalopolis Basin, Peloponnesos, Greece. *Geologica Ultrajectina* 189, 69–92.
- 1131 Vaquero, M., Chacón, M. G., García-Antón, M. D., de Soler, B. G., Martínez, K., Cuartero, F., 2012. Time and space in the formation of lithic assemblages: The example of Abric Romaní Level J. *Quaternary International* 247 (0), 162 – 181.
- 1134 Villa, P., 2004. Taphonomy and stratigraphy in european prehistory. *Before Farming* 2004 (1), 1–20.
1136 URL <https://doi.org/10.3828/bfarm.2004.1.1>
- 1137 Voorhies, M., 1969. Taphonomy and population dynamics of an early pliocene vertebrate fauna, knox county, nebraska. *Contributions to Geology, University of Wyoming Special Paper* 1, 1–69.
- 1140 Walter, M. J., Trauth, M. H., 2013. A {MATLAB} based orientation analysis of acheulean handaxe accumulations in olorgesailie and kariandusi, kenya rift. *Journal of Human Evolution* 64 (6), 569 – 581.

- 1143 Wood, R. W., Johnson, D. L., 1978. A survey of disturbance processes in archaeological
1144 site formation. In: Schiffer, M. B. (Ed.), Advances in archaeological method and
1145 theory. Vol. 1. Academic Press, Ch. 9, pp. 315–381.
- 1146 Woodcock, N., Naylor, M., 1983. Randomness testing in three-dimensional orientation
1147 data. Journal of Structural Geology 5 (5), 539 – 548.